

Accepted Manuscript

X-ray crystal structure guided discovery of new selective, substrate-mimicking sirtuin 2 inhibitors that exhibit activities against non-small cell lung cancer cells

Ling-Ling Yang, Hua-Li Wang, Lei Zhong, Chen Yuan, Si-Yu Liu, Zhu-Jun Yu, Sha Liu, Yu-Hang Yan, Chengyong Wu, Yuxi Wang, Zhouyu Wang, Yamei Yu, Qiang Chen, Guo-Bo Li

PII: S0223-5234(18)30532-4

DOI: [10.1016/j.ejmech.2018.06.041](https://doi.org/10.1016/j.ejmech.2018.06.041)

Reference: EJMECH 10511

To appear in: *European Journal of Medicinal Chemistry*

Received Date: 3 May 2018

Revised Date: 12 June 2018

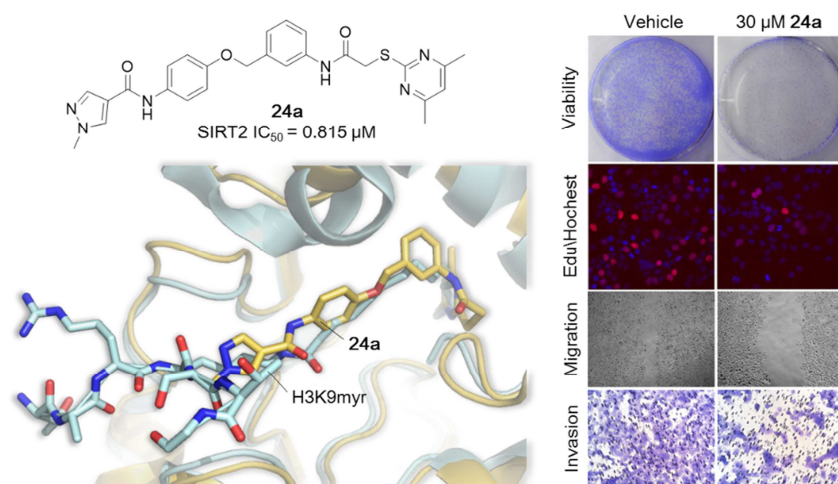
Accepted Date: 15 June 2018

Please cite this article as: L.-L. Yang, H.-L. Wang, L. Zhong, C. Yuan, S.-Y. Liu, Z.-J. Yu, S. Liu, Y.-H. Yan, C. Wu, Y. Wang, Z. Wang, Y. Yu, Q. Chen, G.-B. Li, X-ray crystal structure guided discovery of new selective, substrate-mimicking sirtuin 2 inhibitors that exhibit activities against non-small cell lung cancer cells, *European Journal of Medicinal Chemistry* (2018), doi: 10.1016/j.ejmech.2018.06.041.

This is a PDF file of an unedited manuscript that has been accepted for publication. As a service to our customers we are providing this early version of the manuscript. The manuscript will undergo copyediting, typesetting, and review of the resulting proof before it is published in its final form. Please note that during the production process errors may be discovered which could affect the content, and all legal disclaimers that apply to the journal pertain.



Graphical Abstract



**X-ray Crystal Structure Guided Discovery of New Selective,
Substrate-Mimicking Sirtuin 2 Inhibitors That Exhibit Activities against
Non-small Cell Lung Cancer Cells**

Ling-Ling Yang^{†,‡,¶}, Hua-Li Wang^{†,¶}, Lei Zhong^{§,¶}, Chen Yuan[‡], Si-Yu Liu[‡], Zhu-Jun Yu[†], Sha Liu[†], Yu-Hang Yan[†], Chengyong Wu[†], Yuxi Wang[†], Zhouyu Wang[‡], Yamei Yu[†], Qiang Chen^{*,†}, Guo-Bo Li^{*,†}

[†] *Key Laboratory of Drug Targeting and Drug Delivery System of Ministry of Education, West China School of Pharmacy, and State Key Laboratory of Biotherapy and Cancer Center, West China Hospital, West China Medical School, Sichuan University, Chengdu 610041, China.*

[‡] *College of Food and Bioengineering, Xihua University, Sichuan 610039, China*

[§] *Personalized Drug Therapy Key Laboratory of Sichuan Province, Hospital of the University of Electronic Science and Technology of China and Sichuan Provincial People's Hospital, Sichuan 610072, China*

[¶] L.-L. Yang, H.-L. Wang, and L. Zhong contributed equally to this work.

*Corresponding author: liguobo@scu.edu.cn (G.-B. Li); qiang_chen@scu.edu.cn (Q. Chen).

Abstract

Human sirtuin 2 (SIRT2) is a nicotinamide adenine dinucleotide (NAD⁺)-dependent deacylase, and is implicated in human diseases including cancer. Selective small-molecule inhibitors for SIRT2 are sought as chemical tools and potential therapeutics. Here we report the X-ray crystal structure guided structure-activity relationship studies of new *N*-(3-(phenoxyethyl)phenyl)acetamide derivatives with SIRT2, which led to the identification of potent, selective SIRT2 inhibitors. Crystallographic analyses reveal that the new inhibitors act *via* inducing the formation of an enlarged hydrophobic pocket and particularly mimicking the interactions made by myristoylated-lysine substrates. The most potent inhibitor **24a** could dose-dependently elevate the acetylation level of α -tubulin in the non-small cell lung cancer H441 cells, which have a high expression level of SIRT2 as determined by Western blotting analyses. Further cellular assays reveal that **24a** restrains cell growth mainly through inhibiting cellular proliferation rather than inducing apoptosis. Moreover, **24a** could suppress the migration and invasion of H441 cells. These results provide an excellent basis for further development of new potent, selective, and cell active SIRT2 inhibitors as chemical tools and potential therapeutics for SIRT2-driven non-small cell lung cancers.

Introduction

The lysine deacetylases (KDACs) are important epigenetic modification enzymes, which are involved in multiple physiological processes as well as the development and progression of human diseases (*e.g.* cancer).^[1-3] KDACs can be classified into those employing one zinc ion to promote catalysis (termed histone deacetylases, HDACs) and those employing the nicotinamide adenine dinucleotide (NAD⁺) as a cofactor in catalysis (termed sirtuins, SIRTs) (Figure 1a).^[3] Several clinically useful inhibitors for the HDACs, including Vorinostat, Romidepsin, Chidamide, Panobinostat, and Belinostat, have been established for treating cutaneous T cell lymphoma, peripheral T-cell lymphoma or multiple myeloma. In contrast, there are no such inhibitors for the sirtuins.^[1]

The human genome encodes seven isoforms of sirtuins (SIRT1-7), which differ in their catalytic activity and subcellular localization (Table S1). Sirtuins are able to erase various acyl groups, such as acetyl, propionyl, crotonyl, succinyl, glutaryl, decanoyl, myristoyl and palmitoyl, from histones and many other protein substrates;^[4,5] nevertheless, sirtuin isoforms exhibit different preference for acyl-lysine substrates (Table S1). The SIRT2, mainly located in cytoplasm, can catalyze deacetylation and defatty-acylation for various protein substrates, including transcription factors (*e.g.*, p53, Foxo1, p300, NFκB, and HIF1α), differentiation proteins (*e.g.*, tubulin, keratin 8, PAR3, and PRLR), and metabolic enzymes (*e.g.*, G6PD, LDH, PEPCK1, S6K1, and PGAM).^[2,5,6] The dysregulation or overexpression of SIRT2 is often described as a key factor contributing to human diseases, including

cancers. For example, Chen *et al* found that SIRT2 was overexpressed in hepatocellular carcinoma cell lines, and it promoted epithelial to mesenchymal transition *via* the deacetylation of protein kinase B and the activation of the glycogen synthase kinase-3 β / β -catenin signaling pathway.^[7] SIRT2 was also observed to be up-regulated in pancreatic adenocarcinoma and breast cancer, and SIRT2 deletion or inhibition led to the suppression of cancer cell growth, invasion, and metastasis.^[8-10] Thus, the development of potent and selective SIRT2 inhibitors would be an impetus to investigate associated molecular mechanisms and to develop potential agents combating cancer or other relevant diseases.

To date, a number of structurally diverse small-molecule SIRT2 inhibitors have been reported (Figure S1).^[11-20] Notably, aminothiazoles and thienopyrimidinones were discovered as new types of selective SIRT2 inhibitors, which work *via* inducing the formation of an allosteric hydrophobic binding pocket, hence providing new insights into inhibitor design.^[21-24] With the aid of LEADOPT,^[25] an automatic structure-based molecule design tool, we successfully identified the *N*-(3-(phenoxy)methyl)phenyl)acetamide derivatives (Figure 1b and Figure S2) as selective SIRT2 inhibitors, which exhibited inhibitory activity against human breast cancer cell growth.^[26] Here we describe the X-ray crystal structure guided structure-activity relationship (SAR) studies of new *N*-(3-(phenoxy)methyl)phenyl)acetamide derivatives and their activities against non-small cell lung cancer.

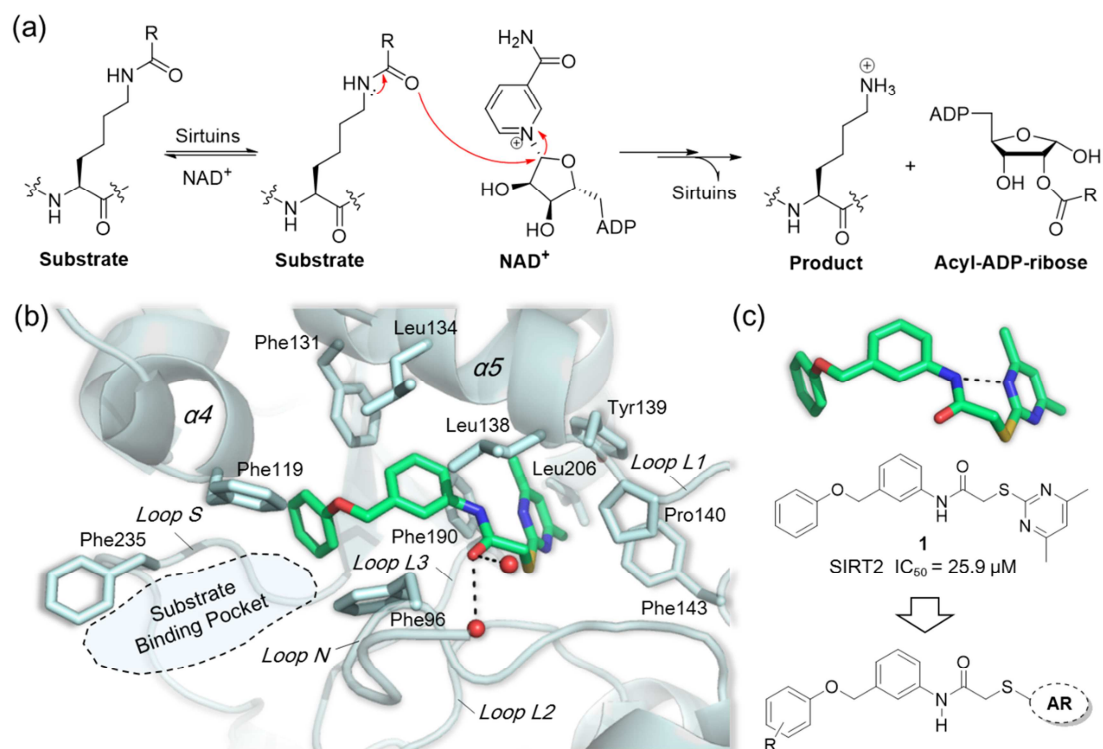


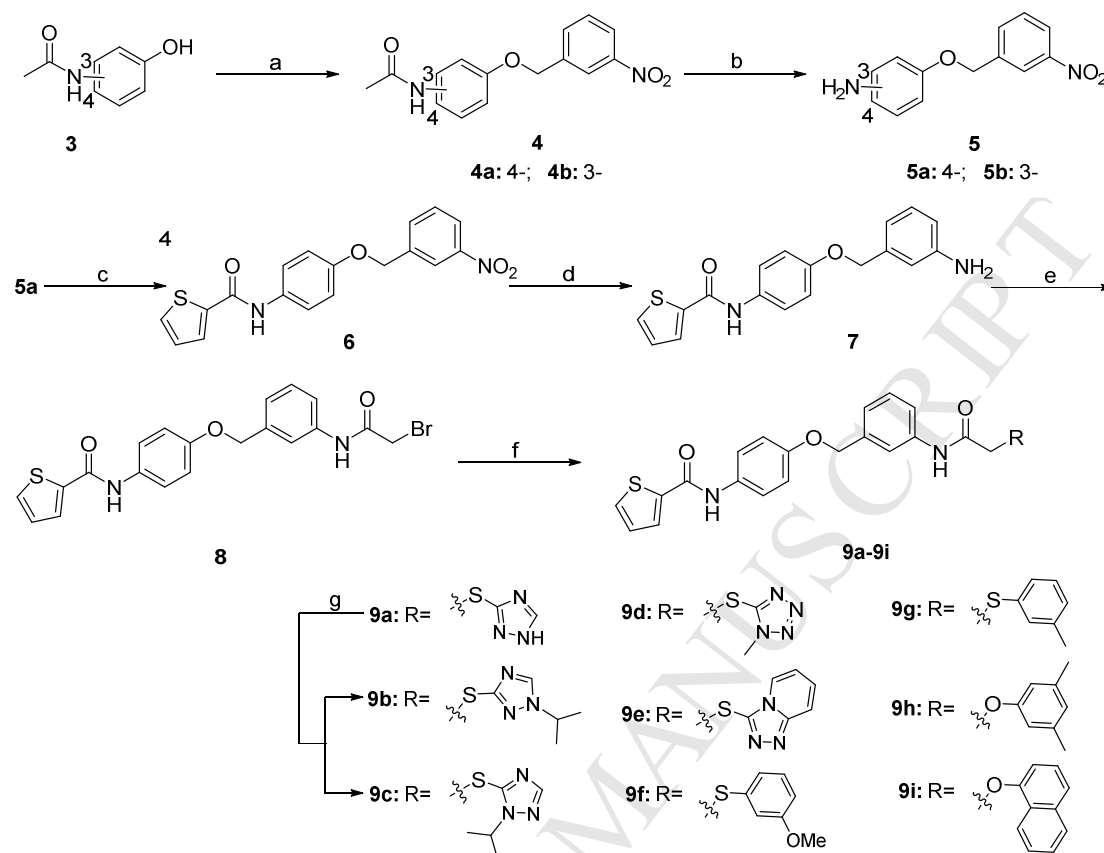
Figure 1. Crystallographic analysis reveals the binding mode of **1** with SIRT2. (a) Outline mechanisms for sirtuin catalysed deacylations. (b) View from the SIRT2:**1** complex structure (PDB ID 5YQL) showing that **1** binds to make hydrophobic interactions with residues Phe119, Phe131, Leu134, Leu138, Leu206, Tyr139, Pro140, Phe190, Phe96, and Phe143. (c) Schematic showing aromatic rings (AR) or R-substituents on the *N*-(3-(phenoxy)methyl)phenylacetamide scaffold that were the focus of structural modifications.

We first carried out the crystallographic analyses of SIRT2 with 2-((4,6-dimethylpyrimidine-2-yl)thio)-*N*-(3-(phenoxy)methyl)phenylacetamide (**1**), which reveal that similar to aminothiazoles and thienopyrimidinones, **1** induces the formation of an enlarged hydrophobic pocket at the interface of the Rossmann fold domain and the Zn-binding domain (Figure 1b and Figure S2), but which does not occupy the substrate-lysine binding pocket (Figure 1b), suggesting that there is still a considerable possibility for structural optimization. Therefore, we designed and synthesized a series of new derivatives of **1**, and performed SAR studies with them,

which led to the discovery of new potent SIRT2 inhibitors. The subsequent crystallographic analyses revealed that the new inhibitors bound in the induced hydrophobic pocket, and mimicked the interactions made by the myristoylated-lysine substrates. Since there are few reports of SIRT2 inhibitors against non-small cell lung cancer (NSCLC), we examined the anti-NSCLC effects for the most potent inhibitor.

Chemistry.

A series of new *N*-(3-(phenoxy)methyl)phenyl)acetamide derivatives were synthesized according to the synthetic routes outlined in Schemes 1-3. Briefly, commercially available *N*-(4-hydroxyphenyl)acetamide or *N*-(3-hydroxyphenyl)acetamide (**3**) underwent a five-step process involving K_2CO_3 -promoted nucleophilic substitution, $SOCl_2$ -mediated deacetylation reaction, condensation reaction of acyl halide with amine, Fe-mediated reduction reaction of aromatic nitro compound, and condensation reaction of carboxylic acid with amine to yield the key intermediate **8** in high yield (Scheme 1), which were described in our previous work.^[26] Reactions of the key intermediate **8** with commercially available nucleophiles (*e.g.* aromatic thiol and phenolic hydroxyl) or synthesized nucleophile ([1,2,4]triazolo[4,3-*a*]pyridine-3-thiol, see Scheme S1) in the presence of potassium tert-butoxide as acid binding agent to afford the desired target compounds **9a** and **9d-9i**. Compound **9a** was further reacted with 2-bromopropane to produce the target compounds **9b** (45% yield) and **9c** (36% yield).

Scheme 1. Syntheses of compounds **9a-9i**.^a

^a Reagents and conditions: (a) 1-(bromomethyl)-3-nitrobenzene, K_2CO_3 , DMF, RT, 4h, 81%; (b) $SOCl_2$, MeOH, $65^\circ C$, 3h, 100%; (c) thiophene-2-carbonyl chloride, Et_3N , DCM, $0^\circ C$, 2h, 70%; (d) Fe, NH_4Cl , EtOH/ H_2O =2:1, $90^\circ C$, 1.0h, 92%; (e) 2-bromoacetic acid, HOBT, EDCI, DIPEA, DCM, RT, 12h, 67%; (f) *t*-BuOK, DMF, RT, 3-6h, 30-81%; (g) 2-bromopropane, K_2CO_3 , DMF, $60^\circ C$, 4h, 45% for **9b**, 36% for **9c**.

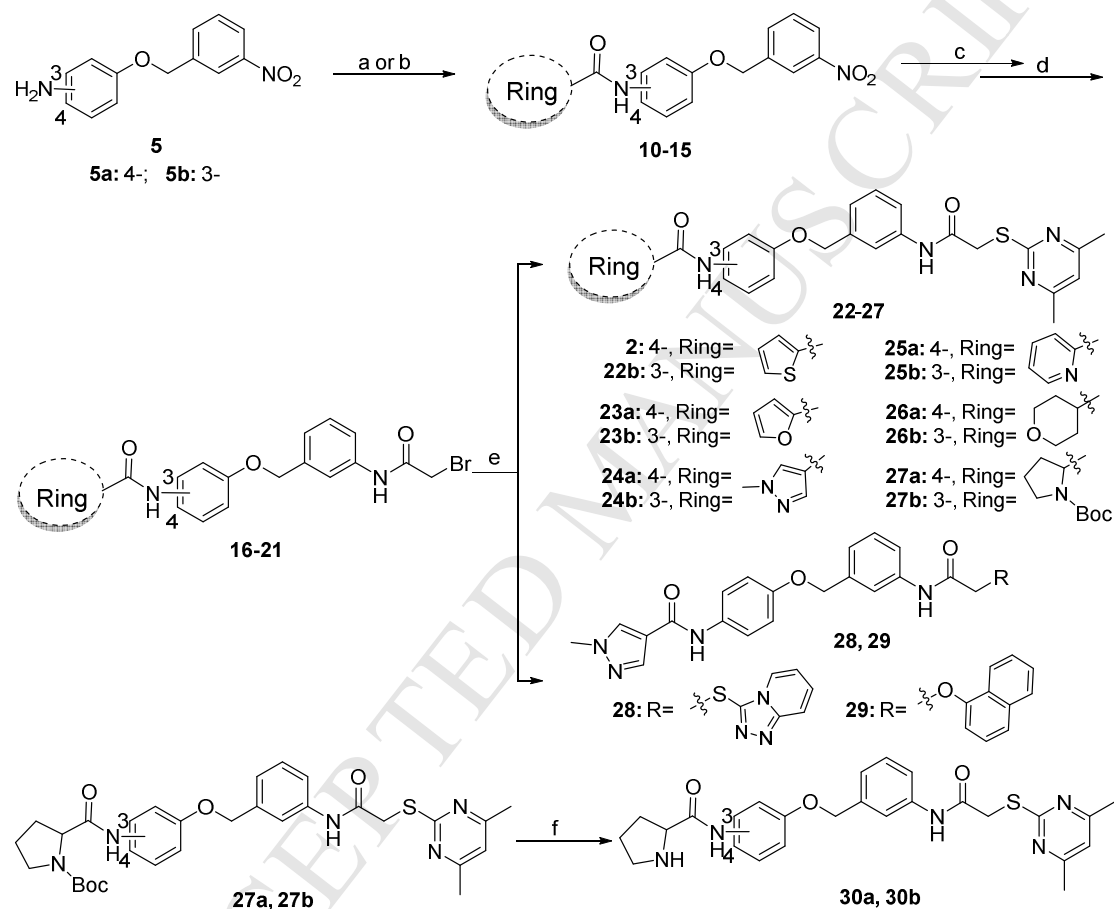
Synthetic access to structurally diverse *N*-(3-(phoxymethyl)phenyl)acetamide derivatives **22-30** was achieved using the similar method as that for compound **2**.^[26] The desired target compounds were prepared in a four-step sequence starting from the synthetic intermediates **5a** or **5b** (see Scheme 2). Firstly, the 3- or 4- free amino group of **5a** or **5b** was transformed to amide group derivatives **10-15** by the standard condensation reaction of acyl halide/carboxylic acid with amine (Scheme 2). Then, Fe-mediated reduction reaction was performed to reduce the nitro group of

intermediates **10-15** to the corresponding amines, followed by coupling with 2-bromoacetic acid to give the key intermediates **16-21**. Finally, nucleophilic substitution of **16-21** with 4,6-dimethylpyrimidine-2-thiol provided the target compounds **22-27** in good overall yields (Scheme 2). Similarly, coupling of *N*-(4-((3-(2-bromoacetamido)benzyl)oxy)phenyl)-1-methyl-1*H*-pyrazole-4-carboxamide (**18a**) with [1,2,4]triazolo[4,3-*a*]pyridine-3-thiol or naphthalen-1-ol in the presence of potassium tert-butoxide at room temperature afforded the desired compounds **28** and **29**. The target compounds **30a** and **30b** were further prepared by removal of the *N*-Boc protecting group of **27a** and **27b** in the presence of trifluoroacetic acid at room temperature, respectively.

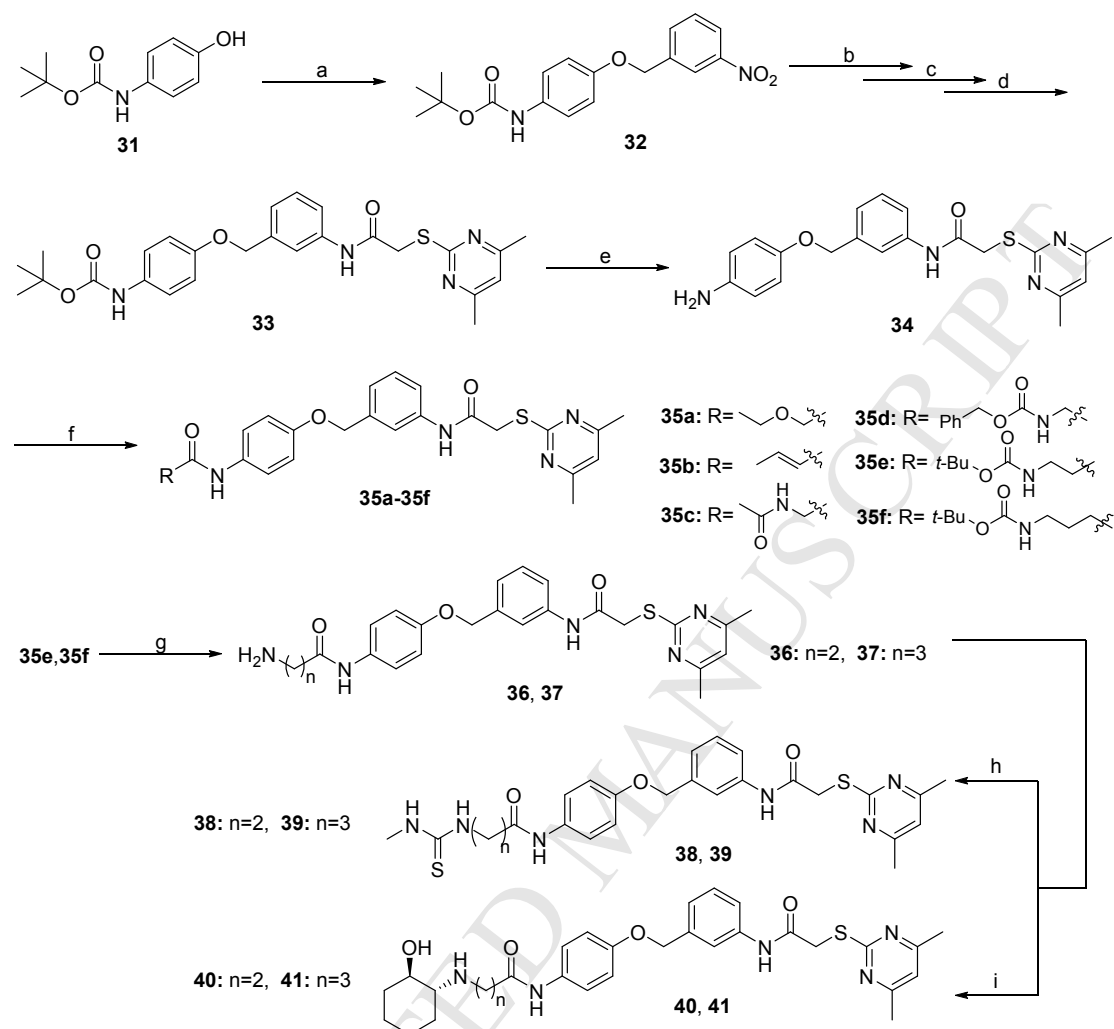
The target compounds **33**, **35a-35f** and **36-41** were prepared as described in Scheme 3. The commercially available tert-butyl(4-hydroxyphenyl)carbamate (**31**) was subjected to the same synthetic transformations as shown in Scheme 1 to afford the target compound **33** in four steps in 52% over yield. Subsequently, **33** was converted to the corresponding intermediate **34** by removing the *N*-Boc protecting group, which was then reacted with different acyclic carboxylic acids to afford the target compounds **35a-35f** in good yields (Scheme 3). The *N*-Boc protecting group of **35e** and **35f** was further removed to give the target compounds **36** (92% yield) and **37** (90% yield), respectively (Scheme 3). The 1-methylthiourea analogues **38** and **39** were synthesized through the condensation reactions of **36** and **37** with isothiocyanatomethane, respectively, in the presence of triethylamine at room temperature (Scheme 3). Finally, the (1*R*,2*R*)-2-aminocyclohexan-1-ol group was

introduced to the free amino group of **36** and **37** under basic conditions using 7-oxabicyclo[4.1.0]heptane to give compounds **40** (48% yield) and **41** (41% yield), respectively (Scheme 3).

Scheme 2. Syntheses of compounds **22-30**.^a



^a Reagents and conditions: (a) Different acyl chlorides, Et₃N, DCM, 0°C, 2h-4h, 70-75%; (b) Different carboxylic acids, HOBT, EDCI, DIPEA, DCM, RT, 12h, 65-78%; (c) Fe, NH₄Cl, EtOH/H₂O =2:1, 90°C, 0.5-2.0 h, 90-96%; (d) HOBT, EDCI, DIPEA, DCM, 2-Bromoacetic acid, RT, 12h, 67%-70%; (e) t-BuOK, DMF, RT, 3-6h, 78-81%; (f) TFA, DCM, RT, 4h, 85% for **30a**, 88% for **30b**.

Scheme 3. Syntheses of compounds **33**, **35a-35f** and **36-41**.^a

^a Reagents and conditions: (a) 1-(bromomethyl)-3-nitrobenzene, K_2CO_3 , DMF, RT, 4h, 87%; (b) Fe, NH_4Cl , $\text{EtOH}/\text{H}_2\text{O} = 2:1$, 90°C , 1.0 h, 93%; (c) 2-bromoacetic acid, HOBT, EDCI, DIPEA, DCM, RT, 12h, 82%; (d) 4,6-dimethylpyrimidine-2-thiol, *t*-BuOK, DMF, RT, 5h, 78%; (e) TFA, DCM, RT, 4h, 95%; (f) Different carboxylic acids, HOBT, EDCI, DIPEA, DCM, RT, 12h, 70-86%; (g) TFA, DCM, RT, 3.5h, 92% for **36**, 90% for **37**; (h) isothiocyanatomethane, Et_3N , DCM, RT, 12h, 80% for **38**, 81% for **39**; (i) 7-oxabicyclo[4.1.0]heptane, Et_3N , H_2O , RT, 12h, 48% for **40**, 41% for **41**.

Results and Discussion

X-ray Crystal Structure Guided SAR Analyses. We began by performing crystallographic analyses of SIRT2 with the hit compound

2-((4,6-dimethylpyrimidine-2-yl)thio)-*N*-(3-(phenoxyethyl)phenyl)acetamide (**1**, Figure 1b), which was identified by using LEADOPT and had an IC_{50} value of 25.9 μ M against SIRT2; under this assay conditions, the known inhibitor SirReal2 showed IC_{50} of 3.38 μ M (Figure S2). Co-crystallization experiments yielded a high-quality X-ray crystal structure of SIRT2:**1** complex (1.64 Å, PDB ID 5YQL); details of crystallization conditions and structure determinations are given in Experimental section and Table S2. SIRT2:**1** crystallized in the $P12_11$ space group with one molecule per asymmetric unit (ASU) (Table S3). We observed that **1** could be confidently modelled into the clear F_o-F_c density at the interface of the Rossmann fold domain and the zinc binding domain (Figure S3).

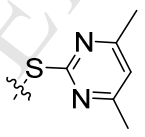
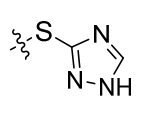
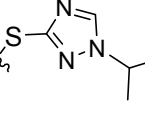
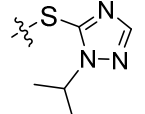
The crystal structure reveals that **1** likely acts as a pseudo-substrate and specifically induces the structural rearrangement of the active site and the formation of the hydrophobic acetyl-lysine-binding tunnel, which is similar as the aminothiazole inhibitors such as SirReal2 (PDB ID 4RMG) (r.m.s.d. of 0.30 Å over 289 C_α atoms, Figure S4)^[22,23]; **1** is positioned to make hydrophobic interactions with Phe96 (loop N), Phe119 (α 4), Phe131 (α 5), Leu134 (α 5), Leu138 (α 5), Tyr139 (α 5), Phe190 (loop L3), Pro140 (loop L1), and Phe143 (loop L1), and π - π stacking interactions with Phe190 (loop L3) (Figure 1b and Figure S5). Comparison of the structures of SIRT2:**1** and SIRT2:H3K9myr (PDB ID 4Y6L)^[27] reveals the binding of **1** may mimic interactions made by the myristoyl moiety of H3K9myr as it binds into the hydrophobic pocket of SIRT2 (Figure S6); nevertheless, **1** does not occupy the substrate binding pocket, *e.g.* where the lysine motif of H3K9myr binds (Figure 1b).

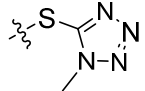
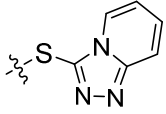
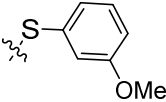
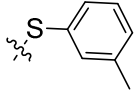
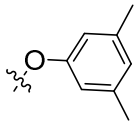
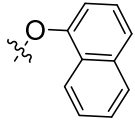
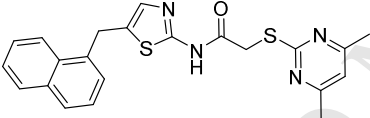
Molecular docking analyses indicate that the compound *N*-(4-((3-(2-((4,6-dimethylpyrimidine-2-yl)thio)acetamido)benzyl)oxy)phenyl)thiophene-2-carboxamide (**2**, Figure S2), which is identified by our preliminary SAR studies,^[26] appears to occupy the substrate binding pocket, thereby leading to more potent inhibition to SIRT2 ($IC_{50} = 3.41 \mu\text{M}$, Figure S2). We attempted co-crystallization but failed to obtain the structure of SIRT2 in complex with **2** (probably due to its poor water solubility). According to the crystallographic and preliminary SAR results, we designed and synthesized a series of new *N*-(3-(phoxymethyl)phenyl)acetamide derivatives (Scheme 1-3) and performed relatively systematic SAR studies for them with SIRT2 (Table 1-3).

Variation of Aromatic Rings to Replace the Dimethylpyrimidine Moiety. As revealed by crystallographic analyses, the dimethylpyrimidine moiety of **1** is positioned to make π - π stacking interactions with Phe190 and hydrophobic interactions with Leu138, Leu206, Phe190, Tyr139, Pro140 and Phe143 (Figure 1b); an intramolecular hydrogen bond between dimethylpyrimidine and amide was observed (Figure 1c), which may contribute to the formation of the preferred binding conformer with the hydrophobic pocket. We therefore used various aromatic rings to replace the dimethylpyrimidine moiety, and synthesized compound **9a-9i** (Table 1) *via* the synthetic routes as shown in Scheme 1. First, 1*H*-1,2,4-triazole (**9a**), 1-isopropyl-1*H*-1,2,4-triazol-3-yl (**9b**), 1-isopropyl-1*H*-1,2,4-triazol-5-yl (**9c**), 1-methyl-1*H*-tetrazole-5-yl (**9d**), and [1,2,4]triazolo[4,3-*a*]pyridine (**9e**) were introduced (Table 1), all of which have potential to form an intramolecular hydrogen

bond with the amide. Comparing with **2**, although these compounds have improved clogP and clogS properties, they showed much lower inhibitory activities to SIRT2 (Table 1 and Figure S7). Similarly, the introduced moieties including 3-methoxyphenyl (**9f**), 3-methylphenyl (**9g**), 3,5-dimethylphenyl (**9h**), and 1-naphthalene (**9i**) led to reduced inhibitory activity (Table 1 and Figure S7). These results indicate that the dimethylpyrimidine moiety is an optimal substituent for further structural optimization.

Table 1. Inhibitory activities and calculated clogP/clogS values of compounds with various aromatic rings to replace the dimethylpyrimidine moiety of the 2-((4,6-dimethylpyrimidine-2-yl)thio)-*N*-phenylacetamide scaffold against human SIRT2.

Cpd. ID	R	Sirt2 (IC ₅₀ (μM) / pIC ₅₀ / s.e. pIC ₅₀) ^a	cLogP ^b	cLogS ^b
2		3.41 / 5.47 / 0.081	5.05	-6.07
9a		>300 / <3.52 / ~	3.57	-5.25
9b		141.6 / 3.85 / 0.096	4.41	-4.68
9c		269.7 / 3.57 / 0.437	4.16	-4.65

9d		44.45 / 4.35 / 0.079	3.27	-4.52
9e		>300 / <3.52 / ~	4.39	-5.95
9f		>300 / <3.52 / ~	5.32	-6.33
9g		>300 / <3.52 / ~	5.60	-6.46
9h		>300 / <3.52 / ~	5.68	-6.61
9i		>300 / <3.52 / ~	6.11	-6.75
SirReal2		3.38 / 5.47 / 0.111	4.63	-5.68

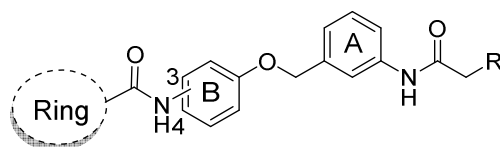
^a The method for measuring IC₅₀ / pIC₅₀ (n=3) values is described in Experimental Section. IC₅₀ curves are given in Figure S7.

^b The clogP and clogS values were calculated using the ALOGPS 2.1 program (<http://www.vcclab.org/lab/alogps/>; available August 5, 2017).^[28]

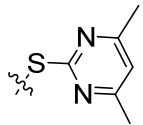
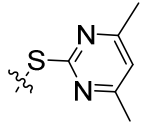
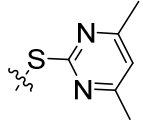
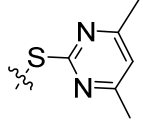
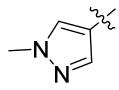
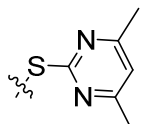
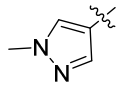
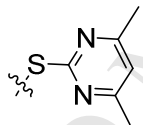
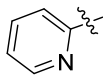
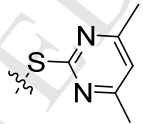
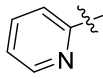
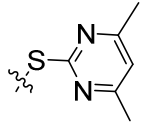
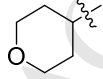
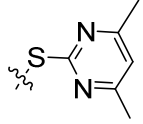
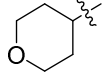
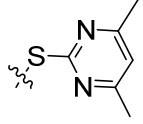
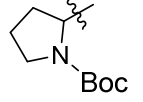
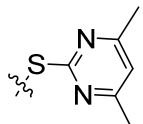
Variation of Cyclic Substituents on 3- or 4-Position of the Phenyl B Moiety. The influence of various cyclic substituents at 3- or 4-position of the phenyl B moiety (Table 2) on the inhibitory activity were then investigated. The compounds **2**, **22b**, **23a-23b**, **24a-24b**, **25a-25b**, **26a-26b**, **28-29**, and **30a-30b** were synthesized using the routes shown in Scheme 2. From the calculated clogP and clogS values (Table 2), compounds **24a**, **24b**, **25a**, **25b**, **26a**, **26b**, **30a**, and **30b** appear to have improved physiochemical properties, compared with **2** (cLogP = 5.05 and cLogS = -6.07).

Comparison of the inhibitory activities between the pairs (**2** vs **22b**), (**23a** vs **23b**), (**24a** vs **24b**), (**25a** vs **25b**), (**26a** vs **26b**) and (**30a** vs **30b**) reveals that the compounds with substituents at the 4-position of the phenyl B moiety have much better potency against SIRT2 than that at the 3-position (Table 2). Compounds **23a**, **24a**, and **26a**, which have furan, 1-methyl-1*H*-pyrazole, and tetrahydro-2*H*-pyran at the 4-position of the phenyl B moiety (Table 2), respectively, showed IC_{50} values of 3.10, 0.815, and 1.32 μ M (Table 2 and Figure S8), respectively, better than **2** (IC_{50} = 3.41 μ M, Figure S2) and SirReal2 (IC_{50} = 3.38 μ M, Figure S2). Interestingly, inconsistent with above compound pairs, **27a** and **27b** exhibited IC_{50} of 76.1 and 15.2 μ M, respectively. Comparison of the inhibitory activity of **28** and **29** with **24a** revealed that replacement of the moieties [1,2,4]triazolo[4,3-*a*]pyridine and naphthalene with dimethylpyrimidine led to significant reduction of potency against SIRT2, further reflecting the good compatibility of dimethylpyrimidine with the induced hydrophobic pocket.

Table 2. Inhibitory activities and calculated clogP/clogS values of compounds with various cyclic substituents on 3- or 4-position of the phenyl B moiety against human SIRT2.



ID	Ring	Pos.	R	SIRT2 (IC_{50} (μ M) / pIC_{50} / s.e. pIC_{50}) ^a	cLogP	cLogS
----	------	------	---	--	-------	-------

2		4		3.41 / 5.47 / 0.081	5.05	-6.07
22b		3		127.7 / 3.89 / 0.500	4.99	-6.05
23a		4		3.10 / 5.51 / 0.075	4.66	-4.42
23b		3		122.6 / 3.91 / 0.224	4.59	-4.42
24a		4		0.815 / 6.09 / 0.021	3.52	-5.09
24b		3		93.7 / 4.03 / 0.045	3.48	-5.10
25a		4		29.4 / 4.53 / 0.057	4.23	-5.72
25b		3		>300 / <3.52 / ~	4.19	-5.70
26a		4		1.32 / 5.88 / 0.029	4.08	-5.59
26b		3		168.8 / 3.77 / 0.225	4.03	-5.57
27a		4		76.1 / 4.12 / 0.036	4.31	-5.42

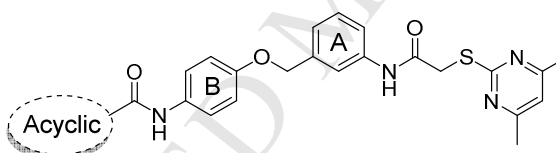
27b		3		15.2 / 4.82 / 0.063	3.92	-5.30
30a		4		41.3 / 4.38 / 0.029	3.18	-5.36
30b		3		141.6 / 3.85 / 0.096	3.13	-5.35
28		4		>300 / <3.52 / ~	3.63	-5.14
29		4		>300 / <3.52 / ~	4.85	-5.48
SirR eal2				3.38 / 5.47 / 0.111	4.63	-5.68

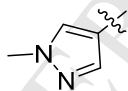
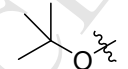
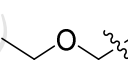
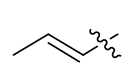
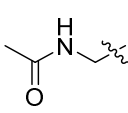
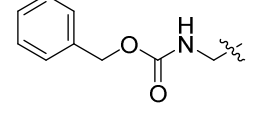
^a The method for measuring IC₅₀ / pIC₅₀ (n=3) values is described in Experimental Section. IC₅₀ curves are given in Figure S8.

Variation of Acyclic Substituents on 4-Position of the Phenyl B Moiety. The inhibitory activities of compounds with various acyclic substituents on 4-position of the phenyl B moiety were also investigated (Table 3). Compounds **33**, **35a**, **35b**, **36** and **37**, bearing the 2-methylpropan-2-ol, methoxyethane, prop-1-ene moiety, ethanamine and propan-1-amine, respectively, showed IC₅₀ of ~100 μM (Table 3 and Figure S9), whereas compounds **35d-35f**, which have larger substituents (*e.g.*, benzyl methylcarbamate, *tert*-butyl ethylcarbamate and *tert*-butyl propylcarbamate, Table 3), displayed lower inhibitory activity to SIRT2 than **33**, **35a**, **35b**, **36** and **37** (Table 3 and Figure S9). Compounds **37** and **38**, bearing the 1-methyl-3-ethylthiourea and

1-methyl-3-propylthiourea moiety at 4-position of the phenyl B moiety, manifested IC_{50} of 11.7 μM and 9.56 μM , respectively (Table 3 and Figure S9), which is less potent than **24a** ($IC_{50} = 0.815 \mu\text{M}$, Table 3). Similar to compounds **35d-35f**, compounds **40** and **41** displayed low inhibitory potency to SIRT2 (Table 3), probably due to the blocking effects of the large substituents at 4-position of the phenyl B moiety. Overall, these SAR results revealed very potent SIRT2 inhibitors (e.g. **24a**), and reflected the high requirements for specific compounds to perfectly bind with the induced hydrophobic pocket.

Table 3. Inhibitory activities and calculated clogP/clogS values of compounds with acyclic substituents on 4-position of the phenyl B moiety against human SIRT2.



ID	Acyclic	SIRT2 (IC_{50} (μM) / pIC_{50} / s.e. pIC_{50}) ^a	cLogP	cLogS
24a		0.815 / 6.09 / 0.021	3.52	-5.09
33		100.2 / 4.00 / 0.027	4.62	-5.74
35a		109.5 / 3.96 / 0.108	3.86	-5.5
35b		89.3 / 4.05 / 0.477	4.68	-5.76
35c		>300 / <3.52 / ~	3.10	-5.34
35d		>300 / <3.52 / ~	4.27	-5.92

35e		~300 / ~3.52 / ~	4.15	-5.73
35f		>300 / <3.52 / ~	4.41	-5.82
36		~300 / ~3.52 / ~	2.55	-5.26
37		70.6 / 4.15 / 0.043	2.83	-5.42
38		11.7 / 4.93 / 0.047	3.61	-5.32
39		9.56 / 5.02 / 0.052	3.89	-5.44
40		>300 / <3.52 / ~	3.35	-5.40
41		175.0 / 3.76 / 0.047	3.62	-5.55

^a The method for measuring IC₅₀ / pIC₅₀ (n=3) values is described in Experimental Section. IC₅₀ curves are given in Figure S9.

Crystallographic Studies. In order to investigate how the most potent inhibitor **24a** (IC₅₀ = 0.815 μM) binds with SIRT2, we sought to obtain the crystal structure of the complex of SIRT2 with **24a**. The SIRT2:**24a** structure was obtained by co-crystallization (crystal conditions see Table S2) and determined to 1.52 Å resolution (Table S3). This structure crystallized in the *P*12₁1 space group with one monomer per asymmetric unit, which is same as the SIRT2:**1** structure (Table S3). We observed that there was clear *F_o-F_c* density at the interface of the Rossmann fold domain and the zinc binding domain (Figure S10), into which **24a** could be

confidently modelled. The crystal structure reveals that **24a** is positioned to make hydrogen-bonding interactions with Val233 (loop S) and Arg97 (loop N), π - π stacking interactions with Phe190 (loop L3) and Phe235 (loop S), and hydrophobic interactions with Phe119 (α 4), Phe131 (α 5), Leu134 (α 5), Leu138 (α 5), Pro140 (loop L1), Phe 143 (loop L1), Ile169 (loop L2), Phe96 (loop N), and Phe235 (loop S) (Figure 2a and Figure S11).

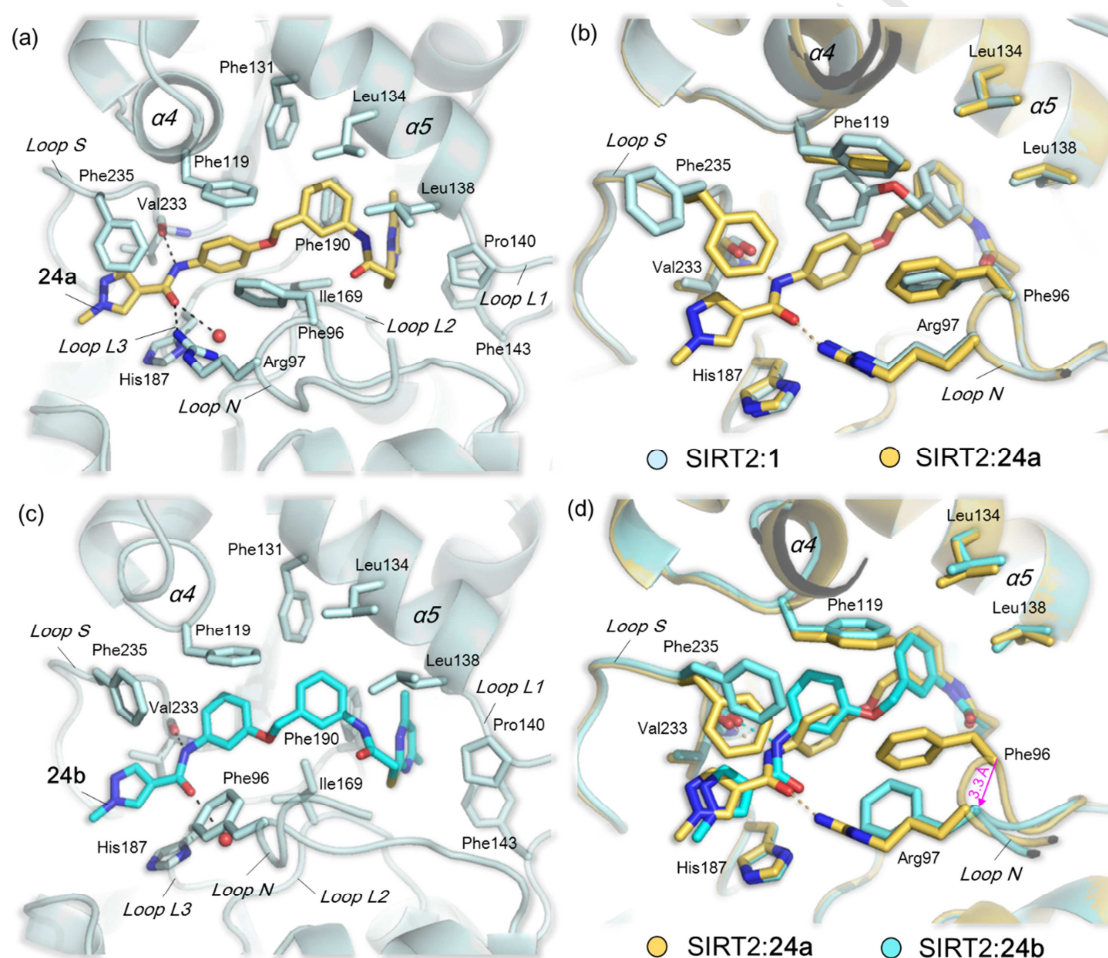


Figure 2. Crystallographic analyses of SIRT2 with **24a** and **24b**. (a) View from a crystal structure of SIRT2:**24a** complex (PDB ID 5YQO) reveals that the inhibitor forms hydrophobic and electrostatic interactions with residues on the α 4/ α 5 helices and the S/N loops. (b) Comparison of complex structures of SIRT2:**1** and SIRT2:**24a** shows that both induce/bind to the hydrophobic pocket. (c) View from a crystal structure of SIRT2:**24b** complex (PDB ID 5YQN) reveals that **24b** binds *via* a similar mode with that of **24a**. (d) **24b** appears not able to induce the formulation of stable

interactions with the loop N, *e.g.*, its binding leads to 3.3 Å movement of the C- α atom of Phe96 (loop N) from that observed in the SIRT2:**24a** structure.

Comparison of structures of SIRT2:**24a** and SIRT2:**1** reveals that **24a** and **1** induce the formation of a similar hydrophobic pocket (r.m.s.d. of 0.08 Å over 286 C α atoms) (Figure 2b and Table S4); the 2-((4,6-dimethylpyrimidine-2-yl)thio)-*N*-phenylacetamide moiety of **24a** and **1** is positioned to make similar hydrophobic interactions with the residues around the induced pocket. Notably, compared with **1**, **24a** is likely able to make more tight interactions with SIRT2, *e.g.* forming hydrophobic interactions with Arg97 and Val233 and π - π stacking interactions and Phe235 (Figure 2a-b), which may explain why **24a** (IC₅₀ = 0.815 μ M) has more potent inhibition to SIRT2 than **1** (IC₅₀ = 25.9 μ M).

We then performed crystallographic analyses for the complex of SIRT2 with **24b**, which has the same moiety as **24a** (*i.e.* 1-methyl-1*H*-pyrazole-4-carboxamide) at 3-position of the phenyl B moiety (Table 2), but has low inhibitory activity to SIRT2 (IC₅₀ = 93.7 μ M). Pleasingly, we obtained a high-resolution SIRT2:**24b** structure (1.63 Å) by co-crystallization experiments (Table S2). The structure reveals that **24b** is positioned to make hydrogen-bonding and hydrophobic interactions with the residues on loops N/S/L1/L2/L3 and helices α 4/ α 5 around the induced hydrophobic pocket, similar as that observed in the SIRT2:**1** and SIRT2:**24a** structures (Figure 1b, Figure 2a-b and Figure S12-13). Nevertheless, **24b** appears not able to perfectly interact with loop N, of which the binding leads to 3.3 Å movement of the C α atom of

Phe96 (loop N) from that observed in the SIRT2:**24a** and SIRT2:**1** structure (Figure 2d and Figure S14), reflecting that the flexibility of the loop N makes a high requirement for inhibitors to accommodate with the hydrophobic pocket. The results may explain why **24b** inhibits SIRT2 less potently than **24a** or **1**.

Comparison of crystal structures of SIRT2:**24a**, SIRT2:**24b**, SIRT2:**1**, SIRT2:SirReal2 (PDB ID 4RMG)^[22], SIRT2:SirReal probe (PDB ID 5DY5)^[21], SIRT2:thienopyrimidinone (PDB ID 5MAT)^[24], SIRT2:H3K9myr (PDB ID 4Y6L)^[27], and SIRT2:ADP-ribose (PDB ID 3ZGV)^[29] reveals that these *N*-(3-(phoxymethyl)phenyl)acetamide inhibitors induce structural rearrangement of the active site (r.m.s.d. of >1.0 Å for C_α atoms comparing with the structures of SIRT2 with H3K9myr and ADP-ribose, Table S4), and reveals evidence for the flexibility in the conformation of the loop N, suggesting that Phe96 and Arg97 (loop N, Figure 2) may be important in capturing these specific inhibitors (Figure 2).

On superimposing the SIRT2:**24a** structure with the crystal structures of SIRT2 complexed with different substrates, we observed that **24a** appears mimic interactions made by the myristoylated-lysine substrates (*e.g.* H3K9myr^[27]) as they bind to SIRT2 (Figure 3 and Figure S15). For example, the 2-((4,6-dimethylpyrimidine-2-yl)thio)-*N*-(3-(phoxymethyl)phenyl)acetamide moiety of **24a** is positioned to make hydrophobic interactions with SIRT2, similar with the myristoyl moiety of H3K9myr observed in the SIRT2:H3K9myr structure (PDB ID 4Y6L)^[27]. More interestingly, the amide of the 1-methyl-1*H*-pyrazole-4-carboxamide moiety of **24a** forms hydrogen-bonding

interactions with Val233, which is likely equivalent to the amide on the lysine side chain of H3K9myr. These results provide insights into inhibitor design, *e.g.*, *via* mimicking the interaction features of the myristoylated-lysine substrates.

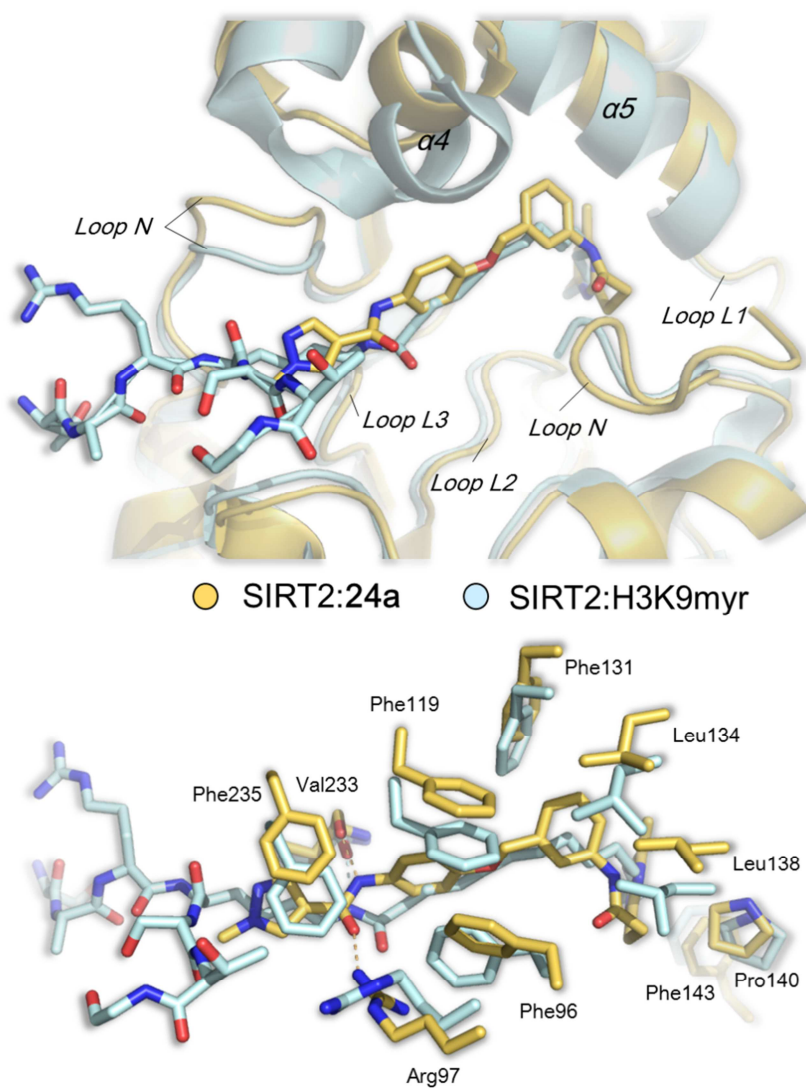


Figure 3. Superimposition of SIRT2:24a (PDB ID 5YQO) with SIRT2:H3K9myr (PDB ID 4Y6L)^[27] revealing that 24a may mimic interactions made by the myristoylated-lysine substrate.

Sirtuin Selectivity Analyses. We then tested the most potent compound 24a against other sirtuin isotypes, including SIRT1, SIRT3, SIRT5, SIRT6, and SIRT7, to investigate its selectivity profiles (see Experimental Section). Notably, no or low

inhibitory activities to all of the tested sirtuin isotypes were observed for **24a** even at the concentration of 100 μM (Table 4). From the structural perspective of sirtuins, SIRT2 has a similar overall domain organization and fold as SIRT1, SIRT3, SIRT4 and SIRT5 (Figure S16), but there are some differences in residues of the catalytic site and $\alpha 4/\alpha 5$ helixes between SIRT2 and other sirtuins;^[30-32] in contrast, SIRT2 has overall domain organization and fold with SIRT6 especially in zinc binding domain and catalytic site (Figure S17).^[30,33] More specially, SIRT2 has a distinct hydrophobic pocket at the interface of the Rossmann fold domain and the zinc-binding domain (near the $\alpha 4$ and $\alpha 5$ helixes and loop N), which can accommodate the myristoylated-lysine substrates^[27] and specific small-molecule inhibitors, such as aminothiazoles,^[21] thienopyrimidinones,^[24] and (3-(phenoxyethyl)phenyl)acetamides (*e.g.* **24a**). These differences may illustrate why **24a** manifests substantial selectivity for SIRT2.

Table 4. The selectivity of **24a** against sirtuin isotypes.

Enzyme	IC ₅₀ (μM)
SIRT2	0.815
SIRT1	>100
SIRT3	>100
SIRT5	>100
SIRT6	>100
SIRT7	>100

Antitumor Activity Studies. Since **24a** has excellent inhibitory potency and selectivity to SIRT2, we used **24a** as a chemical probe to investigate its activities against non-small cell lung cancer (NSCLC) cells; NSCLC cells were chosen here

because there are few reports of SIRT2 inhibitors against this type of cancer. We first detected the expression of SIRT2 in a panel of NSCLC cell lines, including HCC827, H1993, H441, H1975, Calu6, and A549, by Western blot assays. The results reveal that SIRT2 has varied expression levels in the tested NSCLC cell lines (Figure 4a), *e.g.*, having 3.6 times expression level in H441 cells than that in HCC827 cells (Figure 4b), indicating that SIRT2 is likely to have different roles in NSCLC cells.^[34-36]

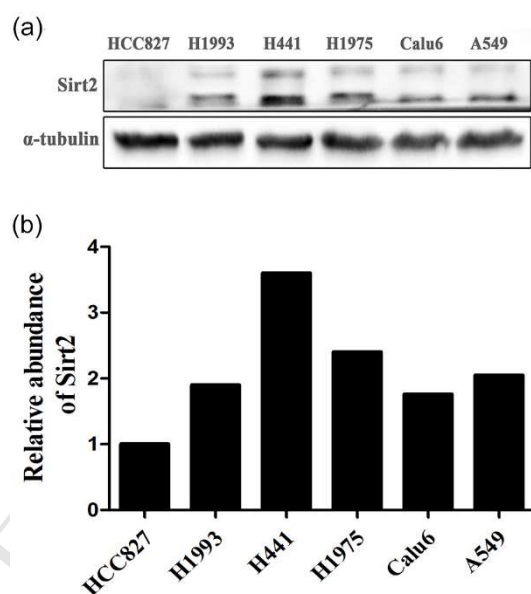


Figure 4. (a) Western blot analyses of SIRT2 expression in a panel of NSCLC cells. (b) SIRT2 abundance was assessed as ratios relative to HCC827 cells normalized to α -tubulin protein loading control.

We then examined whether **24a** is an active inhibitor of SIRT2 in H441 cells, which have a high expression level of SIRT2 (Figure 4), by detecting the acetylation level of α -tubulin, a known protein substrate of SIRT2.^[22,23] As shown in Figure 5, the level of Ac- α -tubulin was dose-dependently elevated in the presence of **24a** in H441

cells, while the structurally similar compound **24b**, which has low potency against SIRT2 (Table 2), had little effects on α -tubulin acetylation; the expression level of Ac- α -tubulin showed a 2.2-fold increase in the presence of **24a** at 30 μ M compared with untreated control, which was set to 1.0. These results indicated that **24a** could suppress the catalytic activity of SIRT2 in H441 cells, and it could be used as a cell-active chemical tool to probe the biological activity of SIRT2 inhibition in H441 cells.

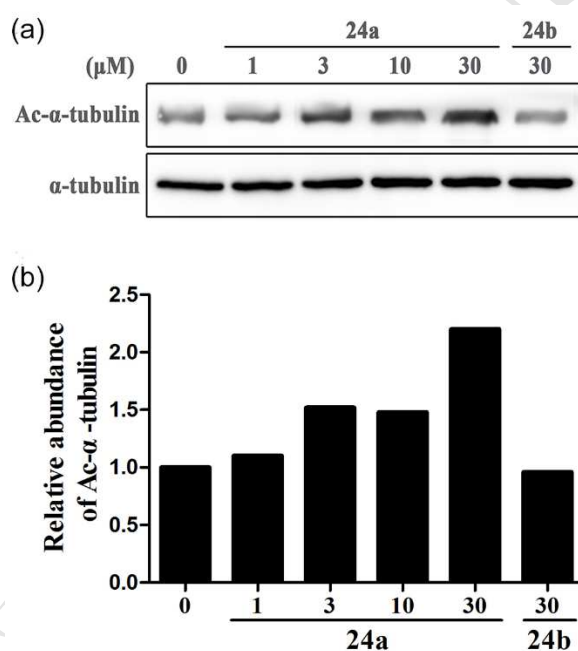


Figure 5. (a) Western blot detection of Ac- α -tubulin levels in H441 cells after 72 h incubation with **24a** or **24b**. (b) Ac- α -tubulin expression was calculated as ratios relative to untreated control normalized to α -tubulin protein loading control.

Anti-viability Activity of 24a. The anti-viability activity of **24a** against H441 cells was tested using MTT assay. The results reveal that **24a** potently inhibited the viability of H441 cells with IC_{50} value of 3.93 μ M (Figure 6a), which is more potent than that of

24b ($IC_{50} > 100 \mu\text{M}$), consistent with their SIRT2 inhibitory activities (Table 2). To complement the results from short-term treatments, long-term colony formation assay was also performed to visually assess the cytoreductive activity of **24a**. As indicated in Figure 6b, **24a** efficiently reduced the formation of colonies at concentrations higher than $3 \mu\text{M}$, while **24b** showed no significant influence on H441 cell colonies.

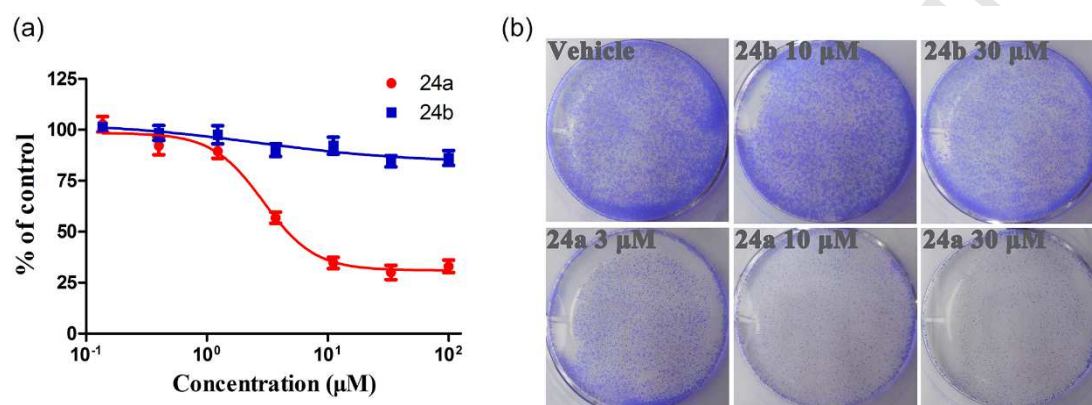


Figure 6. (a) The profile of cell viability after treatment with compound **24a** or **24b**. (b) Long-term colony formation assay on H441 cells.

Anti-proliferation Activity of 24a. We further evaluated the anti-proliferation activity of **24a** using EdU incorporation assays. Compound **24a** could markedly decrease the number of proliferating H441 cells (red nuclei), compared with both DMSO vehicle and **24b** (Figure 7a). Meanwhile, flow cytometry assays were carried out to detect the effects of **24a** on cellular apoptosis. No significant difference in the apoptotic rate of different treatment groups was observed (Figure 7b). These data suggest that **24a** restrains the H441 cell growth mainly through inhibiting cellular proliferation.

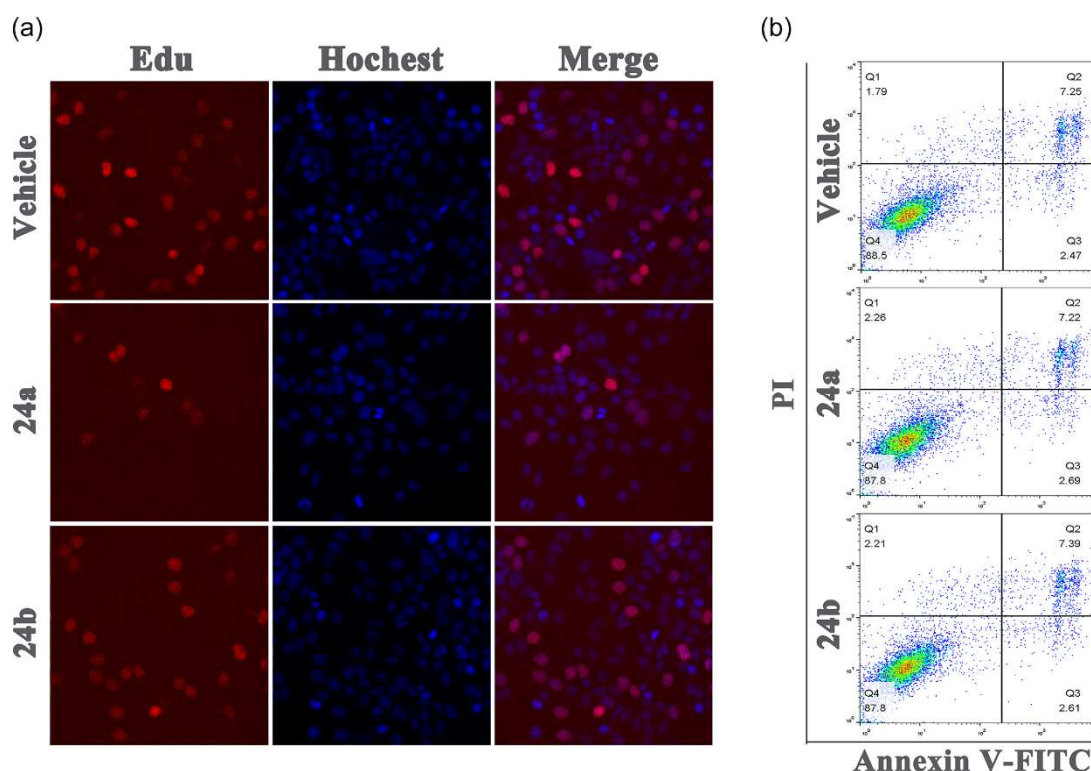


Figure 7. (a) The fluorescence microscopic appearance of EdU and DAPI on H441 cells after treatment with 30 μ M compound **24a** or **24b**. (b) Annexin V/PI co-staining on compound **24a** or **24b** treated H441 cells.

Migration and Invasion Inhibition of 24a. Since it has been reported that SIRT2 is closely related to tumor metastasis,^[7,37,38] we further assessed the ability of **24a** to suppress cell migration and invasion (pivotal steps of tumor metastasis) in H441 cells. In wound healing assay, cell migration was effectively suppressed by **24a** at concentrations higher than 10 μ M (Figure 8). The inhibitory effect was also observed in transwell invasion assays, in which the number of invaded cells was visibly decreased by **24a** in a dose-dependent manner (Figure 8). Of note, compound **24b** showed little activity to inhibit both cell migration and invasion, partly reflecting **24a** works *via* specifically inhibiting SIRT2.

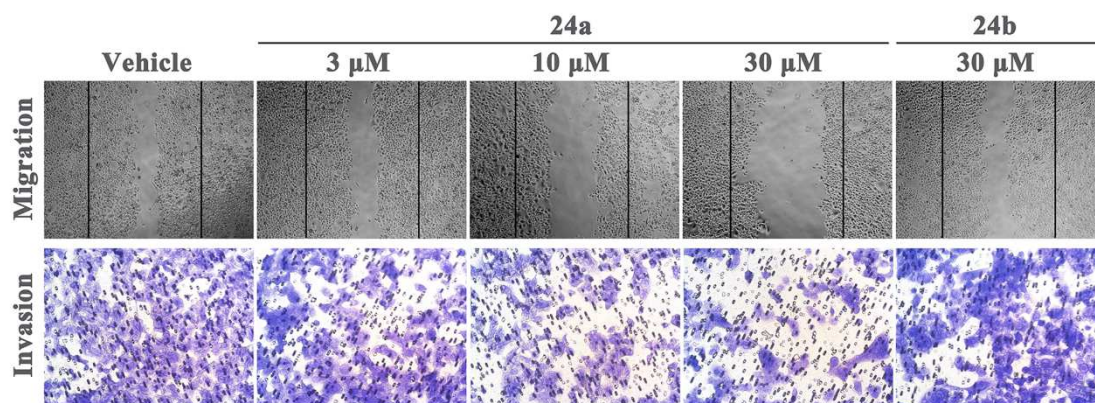


Figure 8. The inhibitory effects of compound **24a** toward H441 cell migration and invasion.

Conclusion.

We described the X-ray crystal structure guided design, synthesis and SAR studies of new *N*-(3-(phenoxy)methyl)phenyl)acetamide derivatives with SIRT2, which led to the identification of potent, selective SIRT2 inhibitors, *e.g.* **24a** with an IC₅₀ value of 0.815 μM. As revealed by crystallographic analyses, **24a** binds with the extended hydrophobic pocket and particularly mimics the interactions made by myristoylated-lysine substrates, providing insights into inhibitor design. Comparison of complex structures of SIRT2 with different inhibitors reveals evidence for flexibility in the conformation of the loop N, suggesting Phe96 and Arg97 may be important in inhibitor capture. Cellular assays reveal that **24a** has the ability to elevate the acetylation level of α-tubulin in dose-dependent manner in H441 NSCLC cell line. Moreover, **24a** could suppress the growth, cell migration and invasion of H441 cells. These results will aid future efforts to develop new potent, selective, and cell active SIRT2 inhibitors, which may provide effective treatments for SIRT2-driven non-small cell lung cancers.

Experimental Section.**Chemistry.**

Unless otherwise stated, the starting materials, reagents, and solvents were obtained from commercial purchase and used as supplied without further purification. Analytical thin-layer chromatography (TLC) was run on Merck silica gel 60 F-254, with detection by UV light ($\lambda = 254\text{nm}$). ^1H and ^{13}C spectra were recorded on a Bruker AV-400 (^1H , 400 MHz; ^{13}C , 100 MHz) instrument at room temperature (rt). Chemical shifts (δ) are expressed in parts per million (ppm) relative to tetramethylsilane (TMS) as an internal standard or the residual solvent peak for ^1H and ^{13}C nucleus (CDCl_3 : $\delta_{\text{H}} = 7.26$, $\delta_{\text{C}} = 77.16$; DMSO-d_6 : $\delta_{\text{H}} = 2.50$, $\delta_{\text{C}} = 39.52$); coupling constants (J values) were given in hertz (Hz). The splitting patterns were described as s (singlet), d (doublet), dd (doublet doublet), t (triplet), q (quartet), m (multiplet), and br (broad). Melting points were measured on an electrothermal melting point apparatus without correction. Low-resolution and high-resolution mass spectral (MS) data were acquired on an Agilent 1100 series LC-MS instrument with UV detection at 254 nm in electrospray ionization (ESI) mode. For all final compounds were purified to >95% purity, as determined by high-performance liquid chromatography (HPLC). HPLC analysis was performed on a Waters 2695 HPLC system equipped with a Kromasil C18 column (4.6 mm \times 250 mm, 5 μm).

General Procedure 1: K_2CO_3 -promoted Nucleophilic Substitution Reaction. A mixture of different substituted phenols (**3** or **31**, 1.05 equiv), 1-(bromomethyl)-3-nitrobenzene (1.0 equiv), and K_2CO_3 (3.0 equiv) in DMF

(1.5mL/mmol) was stirred for 4 h at room temperature. Upon completion of the reaction as determined by TLC, The mixture was partitioned between water and dichloromethane (3×). The organic layer was dried over magnesium sulfate anhydrous, filtered and concentrated in vacuo. The crude products were then recrystallized from ethanol affording the intermediate **4** or **32** with yields ranging from 81% to 87%.

General Procedure 2: SOCl₂-mediated Deacetylation Reaction. To a solution of **4a** or **4b** (1.0 equiv) in methanol (5 mL/mmol), thionyl chloride (0.5 mL/mmol) was added and the mixture was reflux for 3h. Then the reaction was concentrated in vacuo and basified with NaHCO₃ solution (pH 8) and extracted with ethyl acetate (3×), the combined organic extracts were dried (Na₂SO₄), and concentrated under reduced pressure to give 4-((3-nitrobenzyl)oxy)aniline (**5a**) or 3-((3-nitrobenzyl)oxy)aniline (**5b**), which was taken up for the next step without any purification.

General Procedure 3: Fe-participated Reduction Reaction. Iron powder (5 equiv) was added to a solution of nitro compounds **6**, **10-15** or **32** (1 equiv) in EtOH (5mL/mmol) at 50°C-55°C, and then NH₄Cl solution (0.5 equiv in 3 mL/mmol water) was added to the above mixture in succession. Most of the iron powder was filtered while hot after the reaction mixture was refluxed for 0.5-2h, and the filtrate was concentrated under reduced pressure. The residue was basified to PH 7-8 with NaHCO₃ solution and extracted three times with ethyl acetate, the combined organic extracts were dried (Na₂SO₄), and concentrated under reduced pressure to yield the reduction products, which were taken up for the next step without any purification.

General Procedure 4: EDCI-mediated Amide Formation. 2-Bromoacetic acid (1.0

equiv) was reacted with different amines (0.9 equiv) in the presence of 1-hydroxybenzotriazole (HOBT, 1.0 equiv), 1-(3-(dimethylamino)propyl)-3-ethylcarbodiimide hydrochloride (EDCI, 1.0 equiv) and *N,N*-diisopropylethylamine (DIPEA, 1.5 equiv) in CH₂Cl₂ (10 mL/mmol) at room temperature for 12h. Upon completion of the reaction as determined by TLC, The mixture was concentrated and partitioned between water and ethyl acetate (3×). The organic layer was dried over magnesium sulfate anhydrous, filtered and concentrated in vacuo. The products were purified by column chromatography with appropriate eluents.

N-(4-((3-(2-((1*H*-1,2,4-triazol-3-yl)thio)acetamido)benzyl)oxy)phenyl)thiophene-2-carboxamide (**9a**). Using the commercially available *N*-(4-hydroxyphenyl)acetamide (**3a**), the intermediate **5a** was obtained by general procedure 1 and general procedure 2 in turn, which was then reacted with thiophene-2-carbonyl chloride (1.2 equiv) in the presence of Et₃N (3.0 equiv) at 0 °C, in DCM (5 mL/mmol). When TLC indicated that the reaction was finished, the reaction solution was concentrated and the crude product was purified by column chromatography (petroleum ether: EtOAc = 4:1) to give light yellow intermediate **6**, in 70% yield. Next, compound **6** was converted to the key intermediate **8** by the reaction of general procedure 3 and general procedure 4 in turn. Finally, to a mixture of 1*H*-1,2,4-triazole-3-thiol (1.5 equiv) and *t*-BuOK (2.0 equiv) in DMF (5 mL/mmol), intermediate **8** (1.0 equiv) was added, and the reaction mixture was stirred at ambient temperature for 5h. When TLC indicated that the reaction was finished, the reaction mixture was poured into a large amount of water

(20ml/1 ml DMF) and the crude mixture was extracted with ethyl acetate (3×). Then, the combined organic layers were washed with brine, dried, and concentrated. The residue was purified by column chromatography (CH₂Cl₂: MeOH = 40:1) to give the desired target compound **9a**, in 78% yield. 98.6 % HPLC purity. ¹H NMR (400 MHz, DMSO): δ 14.09 (s, 1H), 10.36 (s, 1H), 10.14 (s, 1H), 8.47 (s, 1H), 7.99 (dd, *J*=1.2 Hz, *J*=4.0 Hz, 1H), 7.84 (dd, *J*=1.2 Hz, *J*=4.8 Hz, 1H), 7.70 (s, 1H), 7.64-7.61 (m, 2H), 7.55 (d, *J*=8.0 Hz, 1H), 7.34 (t, *J*=8.0 Hz, 1H), 7.24-7.21 (m, 1H), 7.15 (d, *J*=8.0 Hz, 1H), 7.03-7.00 (m, 2H), 5.08 (s, 2H), 4.07 (s, 2H) ppm. ¹³C NMR (100 MHz, DMSO): δ 166.8, 160.0, 158.7, 155.1, 146.9, 140.7, 139.6, 138.4, 132.4, 132.0, 129.3, 129.2, 128.5, 123.0, 122.5, 118.9, 118.5, 115.3, 69.8, 36.6 ppm. HRMS: *m/z* calcd for C₂₂H₁₉N₅O₃S₂ [M + H]⁺ 466.1018, found 466.1022.

N-(4-((3-(2-((1-isopropyl-1*H*-1,2,4-triazol-3-yl)thio)acetamido)benzyl)oxy)phenyl)thiophene-2-carboxamide (**9b**). A stirring mixture of compound **9a** (150 mg, 0.33 mmol), 2-bromopropane (93 μL, 0.99 mmol), and potassium carbonate (137 mg, 0.99mmol) in DMF (3 mL) was heated to 60°C for 4 h. After this time, the reaction mixture was poured into a large amount of water (80 ml) and extracted with ethyl acetate (3× 100 mL). The combined organic extracts were dried over anhydrous sodium sulfate, filtered, and concentrated under reduced pressure. The residue was purified by column chromatography (CH₂Cl₂: MeOH = 50:1) to give the desired target compound **9b**, in 45% yield. 96.7 % HPLC purity. ¹H NMR (400 MHz, DMSO): δ 10.29 (s, 1H), 10.12 (s, 1H), 8.53 (s, 1H), 7.98 (d, *J*=4.8 Hz, 1H), 7.83 (dd, *J*=0.8 Hz, *J*=4.4 Hz, 1H), 7.68 (s, 1H), 7.61 (d, *J*=8.8 Hz, 2H), 7.53 (d, *J*=8.0 Hz, 1H), 7.32

(t, $J=8.0$ Hz, 1H), 7.21 (t, $J=4.0$ Hz, 1H), 7.13 (d, $J=8.0$ Hz, 1H), 7.00 (d, $J=8.8$ Hz, 2H), 5.07 (s, 2H), 4.55-4.49 (m, 1H), 4.03(s, 2H), 1.39 (d, $J=6.4$ Hz, 6H) ppm. ^{13}C NMR (100 MHz, DMSO): δ 166.9, 160.0, 158.7, 155.1, 143.9, 140.7, 139.6, 138.4, 132.4, 132.0, 129.3, 129.2, 128.5, 123.0, 122.5, 118.9, 118.5, 115.3, 69.7, 52.1, 31.2, 22.6 ppm. HRMS: m/z calcd for $\text{C}_{25}\text{H}_{25}\text{N}_5\text{O}_3\text{S}_2$ $[\text{M} + \text{Na}]^+$ 530.1296, found 530.1290.

N-(4-((3-(2-((1-methyl-1H-tetrazol-5-yl)thio)acetamido)benzyl)oxy)phenyl)thiophene-2-carboxamide (**9d**). The title compound was prepared from intermediate **8** and 1-methyl-1H-tetrazole-5-thiol using the same method of compound **9a**, in 75% yield. 97.2 % HPLC purity. ^1H NMR (400 MHz, DMSO): δ 10.46 (s, 1H), 10.14 (s, 1H), 7.99 (d, $J=3.6$ Hz, 1H), 7.85 (d, $J=4.8$ Hz, 1H), 7.67 (s, 1H), 7.62 (d, $J=8.4$ Hz, 2H), 7.53 (d, $J=8.0$ Hz, 1H), 7.35 (t, $J=8.0$ Hz, 1H), 7.22 (t, $J=4.0$ Hz, 1H), 7.17 (d, $J=8.0$ Hz, 1H), 7.01 (d, $J=8.4$ Hz, 2H), 5.09 (s, 2H), 4.31 (s, 2H), 3.99 (s, 3H) ppm. ^{13}C NMR (100 MHz, DMSO): δ 166.6, 160.4, 157.9, 155.1, 140.6, 139.3, 138.4, 132.7, 132.0, 129.5, 129.2, 128.5, 122.5, 121.2, 118.5, 118.4, 115.3, 69.7, 38.1, 31.2 ppm. HRMS: m/z calcd for $\text{C}_{22}\text{H}_{20}\text{N}_6\text{O}_3\text{S}_2$ $[\text{M} + \text{H}]^+$ 481.2068, found 481.2077.

N-(4-((3-(2-([1,2,4]triazolo[4,3-*a*]pyridin-3-ylthio)acetamido)benzyl)oxy)phenyl)thiophene-2-carboxamide (**9e**). The title compound was prepared from intermediate **8** and [1,2,4]triazolo[4,3-*a*]pyridine-3(2*H*)-thione (**a**₃, the synthetic method see Scheme S1) using the same method of compound **9a**, in 68% yield. 97.2 % HPLC purity. 98.5% HPLC purity. ^1H NMR (400 MHz, DMSO): δ 10.24 (s, 1H), 10.14 (s, 1H), 8.49 (d, $J=7.2$ Hz, 1H), 7.99 (dd, $J=1.2$ Hz, $J=4.0$ Hz, 1H), 7.85-7.83 (m, 2H), 7.64-7.60 (m, 2H), 7.55 (s, 1H), 7.47-7.42 (m, 2H), 7.31 (t, $J=8.0$ Hz, 1H), 7.24-7.21

(m, 1H), 7.14 (d, $J=8.0$ Hz, 1H), 7.09-7.06 (m, 1H), 7.02-6.99 (m, 2H), 5.06 (s, 2H), 3.96 (s, 2H) ppm. ^{13}C NMR (100 MHz, DMSO): δ 166.6, 160.1, 155.1, 151.1, 140.7, 140.0, 139.2, 138.4, 132.4, 132.0, 129.3, 129.2, 129.0, 128.5, 124.7, 123.2, 122.5, 119.1, 118.6, 115.9, 115.3, 114.8, 69.7, 31.17 ppm. HRMS: m/z calcd for $\text{C}_{26}\text{H}_{21}\text{N}_5\text{O}_3\text{S}_2$ $[\text{M} + \text{H}]^+$ 516.1186, found 516.1182; $[\text{M} + \text{Na}]^+$ 538.0986, found 538.0982.

N-(4-((3-(2-(*m*-tolylthio)acetamido)benzyl)oxy)phenyl)thiophene-2-carboxamide (**9g**).

The title compound was prepared from intermediate **8** and 3-methylbenzenethiol using the same method of compound **9a**, in 79% yield. 98.4% HPLC purity. ^1H NMR (400 MHz, DMSO): δ 10.28 (s, 1H), 10.14 (s, 1H), 7.99 (d, $J=3.2$ Hz, 1H), 7.85 (d, $J=5.2$ Hz, 1H), 7.68 (s, 1H), 7.63 (d, $J=8.8$ Hz, 2H), 7.53 (d, $J=8.0$ Hz, 1H), 7.34 (t, $J=8.0$ Hz, 1H), 7.24-7.21 (m, 4H), 7.15 (d, $J=8.0$ Hz, 1H), 7.05-7.00 (m, 3H), 5.08 (s, 2H), 3.86 (s, 2H), 2.28 (s, 3H) ppm. ^{13}C NMR (100 MHz, DMSO): δ 167.4, 160.0, 155.1, 140.7, 139.5, 138.8, 138.4, 136.1, 132.4, 132.0, 129.4, 129.3, 129.0, 128.5, 127.2, 125.6, 123.1, 122.5, 119.0, 118.6, 115.3, 69.7, 37.9, 21.4 ppm. HRMS: m/z calcd for $\text{C}_{27}\text{H}_{24}\text{N}_2\text{O}_3\text{S}_2$ $[\text{M} + \text{H}]^+$ 489.1308, found 489.1322.

N-(3-((3-(2-((4,6-dimethylpyrimidine-2-yl)thio)acetamido)benzyl)oxy)phenyl)

thiophene-2-carboxamide

(**22b**).

First,

N-(3-((3-nitrobenzyl)oxy)phenyl)thiophene-2-carboxamide (**10b**) was prepared according to the synthesis procedure of intermediate **6** (Scheme 1) coupling from commercially available thiophene-2-carbonyl chloride (1.2 equiv) and 3-((3-nitrobenzyl)oxy)aniline (**5b**, 1.0 equiv). Then, compound **10b** was subjected

general procedure 3 and general procedure 4 in turn to give the key intermediate **16b**, and finally, to a stirred mixture of 4,6-dimethylpyrimidine-2-thiol (1.5 equiv) and *t*-BuOK (2.0 equiv) in DMF (5 mL/mmol), the intermediate **16b** (1.0 equiv) was added at room temperature and stirred for 6h. Upon completion of the reaction as determined by TLC, the resulting mixture was extracted by amount of water (20ml/1 ml DMF) with ethyl acetate (3×) and washed with brine, dried, and concentrated to give the crude product, which was purified by column chromatography (CH₂Cl₂: MeOH = 45:1) to give the high-purity target compound **22b**, 98.1% HPLC purity. ¹H NMR (400 MHz, DMSO): δ 10.32 (s, 1H), 10.21 (s, 1H), 8.03 (dd, *J*=0.8 Hz, *J*=2.8 Hz, 1H), 7.88 (dd, *J*=0.8 Hz, *J*=4.0 Hz, 1H), 7.71 (s, 1H), 7.55 (d, *J*=8.4 Hz, 1H), 7.51 (t, *J*=2.0 Hz, 1H), 7.34 (t, *J*=8.0 Hz, 2H), 7.28-7.23 (m, 2H), 7.15 (d, *J*=8.0 Hz, 1H), 6.97 (s, 1H), 6.76 (dd, *J*=1.6 Hz, *J*=6.4 Hz, 1H), 5.09 (s, 2H), 4.05 (s, 2H), 2.33 (s, 6H) ppm. ¹³C NMR (100 MHz, DMSO): δ 169.8, 167.4, 167.1, 160.4, 159.0, 140.5, 140.4, 139.7, 138.3, 132.4, 130.0, 129.6, 129.4, 128.5, 122.8, 119.0, 118.4, 116.5, 113.3, 110.4, 107.6, 69.5, 36.0, 23.8 ppm. HRMS: *m/z* calcd for C₂₆H₂₄N₄O₃S₂ [M + H]⁺ 505.1356, found 505.1367; [M + Na]⁺ 527.1178, found 527.1187;

N-(4-((3-(2-((4,6-dimethylpyrimidine-2-yl)thio)acetamido)benzyl)oxy)phenyl)furan-2-carboxamide (**23a**). Replacing thiophene-2-carbonyl chloride with furan-2-carbonyl chloride, the title compound was prepared using the same method of compound **22b**, 38% yield for four steps. 99.3% HPLC purity. ¹H NMR (400 MHz, DMSO): δ 10.31 (s, 1H), 10.10 (s, 1H), 7.93 (s, 1H), 7.69 (s, 1H), 7.65 (d, *J*=8.8 Hz, 2H), 7.54 (d, *J*=8.4 Hz, 1H), 7.33 (t, *J*=8.0 Hz, 1H), 7.29 (d, *J*=3.6 Hz, 1H), 7.14 (d, *J*=8.0 Hz, 1H),

7.00-6.97 (m, 3H), 6.71-6.70 (m, 1H), 5.07 (s, 2H), 4.05 (s, 2H), 2.33 (s, 6H) ppm. ^{13}C NMR (100 MHz, DMSO): δ 169.8, 167.4, 167.1, 156.4, 155.1, 148.2, 145.9, 139.7, 138.4, 132.2, 129.3, 122.9, 122.5, 119.0, 118.5, 116.5, 115.2, 114.8, 112.6, 69.8, 36.0, 23.8 ppm. HRMS: m/z calcd for $\text{C}_{26}\text{H}_{24}\text{N}_4\text{O}_4\text{S}$ $[\text{M} + \text{H}]^+$ 489.1306, found 489.1325.

N-(4-((3-(2-((4,6-dimethylpyrimidine-2-yl)thio)acetamido)benzyl)oxy)phenyl)-1-methyl-1*H*-pyrazole-4-carboxamide (**24a**). 1-methyl-1*H*-pyrazole-4-carboxylic acid (252mg, 2.0 mmol) was reacted with 4-((3-nitrobenzyl)oxy)aniline (488 mg, 2.0 mmol) in the presence of 1-hydroxybenzotriazole (HOBT, 272 mg, 2.0 mmol), 1-(3-dimethylaminopropyl)-3-ethylcarbodiimide hydrochloride (EDCI, 386 mg, 2.0 mmol), and *N,N*-diisopropylethylamine (DIPEA, 0.58mL, 3.5 mmol) in CH_2Cl_2 (20 mL). The mixture was stirred at room temperature for 12 h. Then, the mixture was concentrated and partitioned between water (80 mL) and ethyl acetate (3×80 mL). The organic layer was dried over magnesium sulfate anhydrous, filtered, concentrated and purified by column chromatography (petroleum ether: EtOAc = 2:1) to give the intermediate **12a** (490 mg) in 69% yield. Using **12a**, the title compound **24a** was obtained by a method similar to that for **23a**. 97.6% HPLC purity. ^1H NMR (400 MHz, DMSO): δ 10.31 (s, 1H), 9.71 (s, 1H), 8.28 (s, 1H), 7.99 (s, 1H), 7.70 (s, 1H), 7.60 (d, $J=8.8$ Hz, 2H), 7.54 (d, $J=8.0$ Hz, 1H), 7.33 (t, $J=8.0$ Hz, 1H), 7.13 (d, $J=7.6$ Hz, 1H), 6.98 (d, $J=7.2$ Hz, 3H), 5.07 (s, 2H), 4.05 (s, 2H), 3.90 (s, 3H), 2.34(s, 6H) ppm. ^{13}C NMR (100 MHz, DMSO): δ 169.8, 167.4, 167.1, 160.6, 154.7, 139.7, 139.2, 138.4, 132.9, 132.8, 129.3, 122.9, 122.0, 119.1, 119.0, 118.6, 116.5, 115.2, 69.8, 39.3, 36.0,

23.8 ppm. HRMS: m/z calcd for $C_{26}H_{26}N_6O_3S$ $[M + Na]^+$ 525.1780, found 525.1682.

N-(4-((3-(2-((4,6-dimethylpyrimidine-2-yl)thio)acetamido)benzyl)oxy)phenyl)picolinamide (**25a**). Replacing 1-methyl-1*H*-pyrazole-4-carboxylic acid with picolinic acid, the title compound was prepared using the same method of compound **24a**, 36% yield for four steps. 97.9% HPLC purity. 1H NMR (400 MHz, DMSO): δ 10.58 (s, 1H), 10.32 (s, 1H), 8.74 (d, $J=3.6$ Hz, 1H), 8.16 (d, $J=7.6$ Hz, 1H), 8.07 (t, $J=7.6$ Hz, 1H), 7.83 (d, $J=8.8$ Hz, 2H), 7.68 (t, $J=6.8$ Hz, 2H), 7.55 (d, $J=8.0$ Hz, 1H), 7.34 (t, $J=8.0$ Hz, 1H), 7.15 (d, $J=7.6$ Hz, 1H), 7.02-6.97 (m, 3H), 5.09 (s, 2H), 4.05 (s, 2H), 2.33 (s, 6H) ppm. ^{13}C NMR (100 MHz, DMSO): δ 169.8, 167.4, 167.1, 162.5, 155.2, 150.6, 148.9, 139.7, 138.6, 138.4, 132.2, 129.3, 127.2, 122.9, 122.7, 122.2, 119.0, 118.6, 116.5, 115.3, 69.8, 36.0, 23.8 ppm. HRMS: m/z calcd for $C_{27}H_{25}N_5O_3S$ $[M + H]^+$ 500.1782, found 500.1689.

N-(4-((3-(2-((4,6-dimethylpyrimidine-2-yl)thio)acetamido)benzyl)oxy)phenyl)tetrahydro-2*H*-pyran-4-carboxamide (**26a**). Replacing 1-methyl-1*H*-pyrazole-4-carboxylic acid with tetrahydro-2*H*-pyran-4-carboxylic acid, the title compound was prepared using the same method of compound **24a**, 35% yield for four steps. 97.5 % HPLC purity. 1H NMR (400 MHz, DMSO): δ 10.30 (s, 1H), 9.88 (s, 1H), 7.68 (s, 1H), 7.55 (d, $J=8.4$ Hz, 1H), 7.42 (s, 1H), 7.33 (t, $J=8.0$ Hz, 1H), 7.21-7.12 (m, 3H), 6.97 (s, 1H), 6.68 (d, $J=7.6$ Hz, 1H), 5.05 (s, 2H), 4.05 (s, 2H), 3.93-3.90 (m, 2H), 3.49-3.44 (m, 2H), 2.62-2.54 (m, 1H), 2.34 (s, 6H), 1.70-1.61 (m, 4H) ppm. ^{13}C NMR (100 MHz, DMSO): δ 173.0, 169.8, 167.4, 167.1, 154.5, 139.6, 138.4, 133.2, 129.3, 122.9, 121.1, 119.0, 118.5, 116.5, 115.3, 69.8, 66.9, 42.1, 35.9, 29.4, 23.8 ppm. HRMS: m/z

calcd for C₂₇H₃₀N₄O₄S [M + Na]⁺ 529.1862, found 529.1882.

Tert-butyl 2-((4-((3-(2-((4,6-dimethylpyrimidine-2-yl)thio)acetamido)benzyl)oxy)phenyl)carbamoyl)pyrrolidine-1-carboxylate (27a). Replacing

1-methyl-1*H*-pyrazole-4-carboxylic acid with (tert-butoxycarbonyl)proline, the title compound was prepared using the same method of compound **24a**, 38% yield for four steps. 97.1 % HPLC purity. ¹H NMR (400 MHz, DMSO): δ 10.30 (s, 1H), 9.84 (s, 1H), 7.68 (d, *J*=10.4 Hz, 1H), 7.55-7.50 (m, 3H), 7.32 (t, *J*=8.0 Hz, 1H), 7.30 (d, *J*=8.0 Hz, 1H), 6.97-6.94 (m, 3H), 5.04 (s, 2H), 4.24-4.14 (m, 1H), 4.05 (s, 2H), 3.45-3.39 (m, 1H), 3.33-3.31 (m, 1H), 2.33 (s, 6H), 2.22-2.15 (m, 1H), 1.93-1.77 (m, 3H), 1.41 (s, 3H), 1.29 (s, 6H) ppm. ¹³C NMR (100 MHz, DMSO): δ 171.5, 169.8, 167.4, 167.1, 154.7, 153.7 139.7, 138.4, 132.9, 129.3, 122.9, 121.2, 119.0, 118.6, 116.5, 115.3, 78.9, 69.7, 60.2, 47.0, 36.0, 31.5, 28.4, 23.9, 23.8 ppm. HRMS: *m/z* calcd for C₃₁H₃₇N₅O₅S [M + H]⁺ 592.2588, found 592.2585.

*N-(4-((3-(2-([1,2,4]triazolo[4,3-*a*]pyridin-3-ylthio)acetamido)benzyl)oxy)phenyl)-1-methyl-1*H*-pyrazole-4-carboxamide (28).* The title compound was prepared from intermediate **18a** and [1,2,4]triazolo[4,3-*a*]pyridine-3(2*H*)-thione (**a**₃, the synthetic method see Scheme S1) using the same method of compound **24a**, in 69% yield. 98.3 % HPLC purity. ¹H NMR (400 MHz, DMSO): δ 10.28 (s, 1H), 9.75 (s, 1H), 8.49 (d, *J*=6.8 Hz, 1H), 8.30 (s, 1H), 8.00 (s, 1H), 7.83 (d, *J*=9.2 Hz, 1H), 7.61 (d, *J*=8.8 Hz, 2H), 7.56 (s, 1H), 7.47-7.42 (m, 2H), 7.30 (t, *J*=8.0 Hz, 1H), 7.13 (d, *J*=8.0 Hz, 1H), 7.07 (t, *J*=6.8 Hz, 1H), 6.97 (d, *J*=9.2 Hz, 2H), 5.04 (s, 2H), 3.96 (s, 2H), 3.89 (s, 3H) ppm. ¹³C NMR (100 MHz, DMSO): δ 166.6, 160.6, 154.7, 151.1, 139.9, 139.2, 139.1,

138.4, 133.0, 129.3, 129.0, 124.7, 123.2, 122.0, 119.1, 118.6, 115.9, 115.2, 114.8, 69.7, 39.3, 39.2 ppm. HRMS: m/z calcd for $C_{26}H_{23}N_7O_3S$ $[M + H]^+$ 514.1680, found 514.1626.

General procedure 5: TFA-catalyzed removal of the *N*-Boc protecting group

To a stirring solution of *N*-Boc compounds (1.0 equiv) in CH_2Cl_2 (25 mL/mmol) was added trifluoroacetic acid (10 equiv) at ambient temperature. The reaction mixture was stirred at room temperature for further 5 h. After completion (monitored by TLC), the solvent was removed in vacuo, the crude residue was treated with 150 mL/1mmol of ice water, and the pH was adjusted to >7-8 with saturated $NaHCO_3$. Then, the water solution was extracted with ethyl acetate (3×). The combined extracts were washed with brine, dried, and concentrated. The crude products were purified by column chromatography with yields ranging from 85% to 95%.

N-(4-((3-(2-((4,6-dimethylpyrimidine-2-yl)thio)acetamido)benzyl)oxy)phenyl)

pyrrolidine-2-carboxamide (30a). The title compound was obtained by the general procedure 5 from compound **27a**. 97.9 % HPLC purity. 1H NMR (400 MHz, DMSO): δ 10.30 (s, 1H), 9.83 (s, 1H), 7.68 (s, 1H), 7.57-7.52 (m, 3H), 7.32 (t, $J=7.6$ Hz, 1H), 7.12 (d, $J=7.6$ Hz, 1H), 6.99-6.91 (m, 3H), 5.05 (s, 2H), 4.04 (s, 2H), 3.68-3.64 (m, 1H), 2.89 (t, $J=6.8$ Hz, 2H), 2.33 (s, 6H), 2.06-1.99 (m, 1H), 1.81-1.72 (m, 1H), 1.68-1.61 (m, 2H) ppm. ^{13}C NMR (100 MHz, DMSO): δ 173.2, 169.8, 167.4, 167.1, 154.7, 139.6, 138.4, 132.5, 129.3, 122.9, 121.1, 119.0, 118.5, 116.5, 115.3, 69.8, 61.2, 47.2, 36.0, 31.0, 26.3, 23.8 ppm. HRMS: m/z calcd for $C_{26}H_{29}N_5O_3S$ $[M + H]^+$ 492.2067, found 492.2058.

Tert-butyl (4-((3-(2-((4,6-dimethylpyrimidine-2-yl)thio)acetamido)benzyl)oxy) phenyl) carbamate (33). Using the commercially available tert-butyl (4-hydroxyphenyl)carbamate (**31**), the title compound **33** was obtained by the procedures as above, 52% yield for four steps. 99.2 % HPLC purity. ¹H NMR (400 MHz, DMSO): δ 10.26 (s, 1H), 9.11 (s, 1H), 7.66 (s, 1H), 7.52 (d, *J*=8.0 Hz, 1H), 7.34-7.29 (m, 3H), 7.10 (d, *J*=8.0 Hz, 1H), 6.96 (s, 1H), 6.89 (d, *J*=9.2 Hz, 2H), 5.01 (s, 2H), 4.03 (s, 2H), 2.32 (s, 6H), 1.46 (s, 9H) ppm. ¹³C NMR (100 MHz, DMSO): δ 169.8, 167.4, 167.1, 153.9, 153.4, 139.6, 138.5, 133.3, 129.3, 122.9, 120.1, 118.9, 118.5, 116.5, 115.3, 79.1, 69.8, 36.0, 28.6, 23.8 ppm. HRMS: *m/z* calcd for C₂₆H₃₀N₄O₄S [M + H]⁺ 495.2056, found 494.2050.

2-((4,6-Dimethylpyrimidine-2-yl)thio)-N-(3-((4-(2-ethoxyacetamido)phenoxy)methyl) phenyl)acetamide (35a). The title compound was obtained by the general procedure 5 and general procedure 4 in turn from compound **33**, 80% yield for two steps. 98.8 % HPLC purity. ¹H NMR (400 MHz, DMSO): δ 10.30 (s, 1H), 9.55 (s, 1H), 7.69 (s, 1H), 7.57-7.53 (m, 3H), 7.32 (t, *J*=8.0 Hz, 1H), 7.13 (d, *J*=8.0 Hz, 1H), 6.97-6.94 (m, 3H), 5.05 (s, 2H), 4.04 (s, 2H), 4.00 (s, 2H), 3.56 (q, *J*=6.8 Hz, 2H), 2.33 (s, 6H), 1.19 (t, *J*=6.8 Hz, 3H) ppm. ¹³C NMR (100 MHz, DMSO): δ 169.8, 168.3, 167.4, 167.1, 154.9, 139.7, 138.4, 132.2, 129.3, 122.9, 121.8, 119.0, 118.5, 116.5, 115.2, 70.3, 69.7, 66.7, 36.0, 23.8, 15.4 ppm. HRMS: *m/z* calcd for C₂₅H₂₈N₄O₄S [M + H]⁺ 481.1903, found 481.1828.

3-Amino-N-(4-((3-(2-((4,6-dimethylpyrimidine-2-yl)thio)acetamido)benzyl)oxy)phenyl) propanamide (36). The title compound was obtained by the general procedure 5 from

compound **35e**, in 92% yield. 98.1 % HPLC purity. ^1H NMR (400 MHz, DMSO): δ 10.32 (s, 1H), 9.97 (s, 1H), 7.70 (s, 1H), 7.55-7.49 (m, 3H), 7.32 (t, $J=8.0$ Hz, 1H), 7.12 (d, $J=8.0$ Hz, 1H), 6.96-6.92 (m, 3H), 5.04 (s, 2H), 4.05 (s, 2H), 3.60 (s br, 2H), 2.91 (t, $J=7.2$ Hz, 2H), 2.46 (t, $J=7.2$ Hz, 2H), 2.33 (s, 6H) ppm. ^{13}C NMR (100 MHz, DMSO): δ 169.9, 169.8, 167.4, 167.1, 154.5, 139.7, 138.4, 133.1, 129.3, 122.9, 121.1, 119.0, 118.6, 116.5, 115.3, 69.8, 38.5, 37.8, 36.0, 23.8 ppm. HRMS: m/z calcd for $\text{C}_{24}\text{H}_{27}\text{N}_5\text{O}_3\text{S}$ [$\text{M} + \text{H}$] $^+$ 466.1985, found 466.2006.

4-Amino-N-(4-((3-(2-((4,6-dimethylpyrimidine-2-yl)thio)acetamido)benzyl)oxy)phenyl)butanamide (37). The title compound was obtained by the general procedure 5 from compound **35f**, in 90% yield. 98.0 % HPLC purity. ^1H NMR (400 MHz, DMSO): δ 10.28 (s, 1H), 9.85 (s, 1H), 7.74 (s br, 2H), 7.69 (s, 1H), 7.51-7.46 (m, 3H), 7.31 (t, $J=10.4$ Hz, 1H), 7.11 (d, $J=10.4$ Hz, 1H), 6.96-6.92 (m, 3H), 5.03 (s, 2H), 4.03 (s, 2H), 2.84 (t, $J=10.4$ Hz, 2H), 2.38 (t, $J=10.4$ Hz, 2H), 2.32 (s, 6H), 1.90-1.81 (m, 2H), 1.37 (m, 9H) ppm. ^{13}C NMR (100 MHz, DMSO): δ 170.3, 169.8, 167.4, 167.2, 154.6, 139.7, 138.4, 133.1, 129.3, 122.9, 121.1, 119.1, 118.6, 116.5, 115.2, 69.8, 38.9, 35.9, 33.3, 31.1, 23.7 ppm. HRMS: m/z calcd for $\text{C}_{25}\text{H}_{29}\text{N}_5\text{O}_3\text{S}$ [$\text{M} + \text{H}$] $^+$ 480.2055, found 480.2067.

N-(4-((3-(2-((4,6-dimethylpyrimidine-2-yl)thio)acetamido)benzyl)oxy)phenyl)-3-(3-methylthioureido)propanamide (38). A solution of compound **36** (89mg, 0.19 mmol), isothiocyanatomethane (40 μL , 0.57 mmol), and Et_3N (80 μL , 0.57 mmol) in CH_2Cl_2 (5 mL) was stirred at room temperature overnight. The solvents were removed under reduced pressure, which yielded the crude title product. Subsequently, the crude

product was purified by column chromatography (CH₂Cl₂: MeOH = 55:1) to give the high-purity target compound **38** (81mg), in 80% yield. 97.6% HPLC purity. ¹H NMR (400 MHz, DMSO) δ 10.27 (s, 1H), 9.81 (s, 1H), 7.68 (s, 1H), 7.53-7.44 (m, 4H), 7.31 (t, *J*=8.0 Hz, 1H), 7.12 (d, *J*=8.0 Hz, 1H), 6.95-6.92 (m, 3H), 5.03 (s, 2H), 4.04 (s, 2H), 3.65 (s br, 2H), 2.81 (s br, 3H), 2.56 (t, *J*=6.4 Hz, 2H), 2.32 (s, 6H) ppm. ¹³C NMR (100 MHz, DMSO): ¹³C NMR (101 MHz, DMSO) δ 169.8, 169.7, 167.8, 167.4, 167.1, 154.6, 139.6, 138.4, 133.1, 129.3, 122.9, 121.1, 119.0, 118.6, 116.5, 115.3, 69.8, 55.4, 36.3, 36.0, 31.1, 23.8 ppm. HRMS: *m/z* calcd for C₂₆H₃₀N₆O₃S₂ [M + H]⁺ 539.1968, found 539.1924.

N-(4-((3-(2-((4,6-dimethylpyrimidine-2-yl)thio)acetamido)benzyl)oxy)phenyl)-4-(3-methylthioureido)butanamide (**39**). The title compound was obtained using a method similar to that for **38**, in 81% yield. 98.2 % HPLC purity. ¹H NMR (400 MHz, DMSO): δ 10.29 (s, 1H), 9.78 (s, 1H), 7.68 (s, 1H), 7.55-7.49 (m, 4H), 7.40 (s br, 1H), 7.32 (t, *J*=8.0 Hz, 1H), 7.12 (d, *J*=8.0 Hz, 1H), 6.97-6.93 (m, 3H), 5.04 (s, 2H), 4.05 (s, 2H), 3.38 (s br, 2H), 2.82 (s br, 3H), 2.34 (s, 6H), 2.31-2.29 (m, 2H), 1.84-1.77 (m, 2H) ppm. ¹³C NMR (100 MHz, DMSO): δ 170.9, 169.8, 168.8, 167.4, 167.1, 154.5, 139.6, 138.4, 133.2, 129.3, 122.9, 121.1, 119.0, 118.5, 116.5, 115.3, 69.8, 49.1, 36.0, 34.1, 31.8, 25.4, 23.8 ppm. HRMS: *m/z* calcd for C₂₇H₃₂N₆O₃S₂ [M + H]⁺ 553.2050, found 553.2046.

N-(4-((3-(2-((4,6-dimethylpyrimidine-2-yl)thio)acetamido)benzyl)oxy)phenyl)-4-(((1*R*, 2*R*)-2-hydroxycyclohexyl)amino)butanamide (**41**). A mixture of compound **37** (48 mg, 0.1 mmol), 7-oxabicyclo[4.1.0]heptane (50 μL, 0.5 mmol), and Et₃N (42 μL, 0.3

mmol) in H₂O (2 mL) was stirred at room temperature overnight. The reaction mixture was adjusted to PH 7 with NH₄Cl solution and extracted with ethyl acetate (3×15mL), the combined organic layer was dried over magnesium sulfate anhydrous, filtered and concentrated *in vacuo*. The residue was then purified by column chromatography (CH₂Cl₂: MeOH = 45:1), which yielded the title compound **41** (23 mg), in 41% yield. 98.0 % HPLC purity. ¹H NMR (400 MHz, DMSO): δ 10.30 (s, 1H), 9.81 (s, 1H), 7.69 (s, 1H), 7.54-7.48 (m, 3H), 7.32 (t, *J*=8.0 Hz, 1H), 7.12 (d, *J*=8.0 Hz, 1H), 6.97 (s, 1H), 6.93 (d, *J*=8.8 Hz, 2H), 5.04 (s, 2H), 4.86 (s br, 1H), 4.04 (s, 2H), 3.19 (s br, 2H), 2.77-2.68 (m, 1H), 2.65-2.58 (m, 1H), 2.36-2.32 (m, 2H), 2.33 (s, 6H), 1.94-1.91 (m, 1H), 1.83-1.74 (m, 3H), 1.62 (s br, 2H), 1.25-1.15 (m, 4H), 1.05-1.00 (m, 1H) ppm. HRMS: *m/z* calcd for C₃₁H₃₉N₅O₄S [M - H]⁻ 576.2650, found 576.2632.

The ¹H NMR and ¹³C NMR spectra of all the compounds are given in Supporting Information Figure S18-S55.

Biological Assays.

Protein Expression and Purification. The recombinant protein SIRT2 (residues 56–356) was expressed in *E. coli* Transetta(DE3) cells (Novagen). A single colony was incubated in LB media supplemented with 34 μg/mL chloramphenicol and 50 μg/mL kanamycin sulfate at 37 °C and 220 rpm. The culture was then transferred to further incubation at 16 °C and 220 rpm until the OD₆₀₀ reached 0.6-0.8. Overexpression was induced by the addition of isopropyl-β-D-thiogalactoside (0.3 mM final

concentration) for 18-24 h at 16°C and 220 rpm. Bacterial cells were collected by centrifugation, and the pellet was resuspended in the lysis buffer A (20 mM Tris-HCl, 250 mM NaCl, and pH 8.0) and then lysed using an ultrahigh-pressure homogenizer (JNBIO). The supernatant was separated from the cellular debris by centrifugation of the lysates at 15,000 rpm for 30 min. The supernatant was applied to a Ni-NTA column (Roche) that were equilibrated in advance with lysis buffer A. The resin was then washed using 20 column volumes of the buffer B (20 mM Tris-HCl, 250 mM NaCl, 10 mM imidazole, and pH 8.0) to remove nonspecifically binding proteins. Then, the SIRT2 proteins were eluted with the buffer C (20 mM Tris-HCl, 250 mM NaCl, 250 mM imidazole, and pH 8.0). The recombinant proteins were pooled, concentrated, and then desalted using a HiTrap Desalting column (GE Healthcare) into the assay buffer (25 mM Tris-HCl, 150 mM NaCl, and pH 8.0) for enzyme kinetic analyses. The SIRT2 proteins were concentrated to 26 mg mL⁻¹ using Amicon Ultra 10K (Millipore) and stored at -80 °C. The SIRT2 proteins for crystallization were further removed the His-Tags using the TEV proteases (1 : 30) in the presence of 0.1% β-mercaptoethanol (β-ME) overnight at 4 °C. The resulted digestions were verified by 12% SDS-PAGE. Uncleaved proteins, His-Tags, and TEV proteases were removed by an Ni-NTA column (HiTrap™, chelating HP, GE Healthcare). The cleaved SIRT2 proteins were then concentrated and further purified by a gel-filtration column (Superdex 75 10/300 GL, GE Healthcare), and eluted at 0.5 mL·min⁻¹ with the buffer (20 mM Tris-HCl 150 mM NaCl, and pH8.0) using an AKTA explorer device (GE Healthcare). Fractions containing the SIRT2 proteins were pooled and

concentrated to 13 mg mL^{-1} and stored at $-80 \text{ }^{\circ}\text{C}$. All purification steps were assessed by 12% SDS-PAGE, and the concentration was determined via a NanoDrop 2000 spectrophotometer (Thermo Scientific).

Human SIRT1 (residues 241-512), human SIRT3 (residues 122-391), human SIRT5 (residues 34-356), human SIRT6 (residues 4-296), and human SIRT7 (residues 68-354) were cloned into a modified pET28 vector containing an N-terminal hexahistidine tag and a TEV protease cleavage site. The SIRT1, SIRT3, SIRT5, SIRT6, and SIRT7 genes were expressed in *E. coli* Transetta(DE3) cells (Novagen) overnight at 16°C . Overexpression was induced with IPTG (0.3 mM) at an OD_{600} of 0.6-0.8. Cells were harvested and resuspended in lysis buffer A (20 mM Tris-HCl , 250 mM NaCl , and $\text{pH } 8.0$ for SIRT1, SIRT3, and SIRT5; 20 mM Tris-HCl , 250 mM NaCl , 0.5 mM TCEP , $\text{pH } 8.0$ for SIRT6; 20 mM Tris-HCl , 250 mM NaCl , $14 \text{ mM } \beta\text{-ME}$ $\text{pH } 8.0$ for SIRT7). The cells were then lysed using an ultrahigh-pressure homogenizer (JNBIO), and debris was removed via centrifugation at $15,000 \text{ rpm}$ for 30 min . The resulting supernatant was loaded onto a Ni-NTA column (Roche), washed with 20 column volumes of the buffer B (20 mM Tris-HCl , 250 mM NaCl , 10 mM imidazole , and $\text{pH } 8.0$ for SIRT1, SIRT3, SIRT5; 20 mM Tris-HCl , 250 mM NaCl , 10 mM imidazole , 0.5 mM TCEP , and $\text{pH } 8.0$ for SIRT6; 20 mM Tris-HCl , 250 mM NaCl , 10 mM imidazole , $14 \text{ mM } \beta\text{-ME}$ $\text{pH } 8.0$ for SIRT7) to remove non-specifically binding proteins. The bound proteins were eluted with buffer C (20 mM Tris-HCl , 250 mM NaCl , 250 mM imidazole , and $\text{pH } 8.0$ for SIRT1, SIRT3, and SIRT5; 20 mM Tris-HCl , 250 mM NaCl , 250 mM imidazole , 0.5 mM TCEP , and $\text{pH } 8.0$ for SIRT6; 20

mM Tris-HCl, 250 mM NaCl, 14 mM β -ME pH 8.0 for SIRT7). Recombinant proteins were concentrated and desalted using a HiTrap Desalting column (GE Healthcare) into the assay buffer for enzyme kinetic analyses (SIRT1 and SIRT3: 20 mM Tris-HCl, 200 mM NaCl, 5% glycerol 5 mM β -ME pH 8.0; SIRT5: 20 mM Tris-HCl, 150 mM NaCl, 5% glycerol pH 8.0; SIRT6: 20 mM Tris-HCl, 150 mM NaCl, 5% glycerol 0.5mM TCEP pH 8.0; SIRT7: 20 mM Tris-HCl, 150 mM NaCl, 5% glycerol, 14 mM β -ME pH 8.0). The proteins were concentrated to 16 mg·mL⁻¹ using Amicon Ultra 10K and stored at 80 °C. The purity of recombinant proteins was validated by SDS-PAGE (>90%).

Inhibition Assays. The activity assays were established based on the internally quenched fluorescent substrates AcIQF and GluIQF (Figure S56). These two substrates were synthesized by DGpeptidesCo., Ltd. More details about the activity assays and the crystal structure of AcIQF in complex with SIRT2 will be reported somewhere. In the activity assays, all enzymes, cofactor NAD⁺ (purchased from Sigma-Aldrich), and substrates were dissolved in the assay buffer; note, sirtuin variations of the assay buffer are described above. All determinations were carried out in black 96-well microtiter plates with a reaction volume of 60 μ L per well. Fluorescence intensity was measured using a Thermo microplate reader ($\lambda_{\text{ex}} = 320$ nm, $\lambda_{\text{em}} = 420$ nm).

Activity Test for Sirtuins with Substrates. Reaction mixtures of the enzymes (SIRT1, SIRT2, SIRT3, SIRT5, SIRT6, or SIRT7: 0.2 μ M) with substrates (AcIQF or GluIQF: 5 μ M or 50 μ M) and NAD⁺ (200 μ M) were incubated for 2 h at 25 °C and 140 rpm.

Then, a stop solution (50 μL) containing $\sim 2 \text{ U}\cdot\mu\text{L}^{-1}$ trypsin (purchased from Sigma-Aldrich) and 4 mM nicotinamide was added to stop the reactions, followed by further incubation for 30 min at 25 $^{\circ}\text{C}$ and 140 rpm. Then, the fluorescence was obtained using a microplate reader.

Inhibitory Activity Test for Compounds with SIRT2. The inhibitory activities of the synthesized compounds against SIRT2 were determined using the AcIQF substrate. The SIRT2 enzymes (0.2 μM) was incubated with each compound (300 μM \sim 15 nM in 3-fold dilution series with final DMSO concentration \leq 1%) for 30 minutes at 25 $^{\circ}\text{C}$, followed by adding AcIQF (5 μM) and NAD^{+} (200 μM) to start the reactions and incubate for 2 h at 25 $^{\circ}\text{C}$. Then, a stop solution (50 μL) containing $\sim 2 \text{ U}\cdot\mu\text{L}^{-1}$ trypsin and 4 mM nicotinamide was added to stop the reactions. After further incubation for 30 minutes, the fluorescence was recorded. All determinations were tested in triplicate. The IC_{50} / pIC_{50} / s.e. pIC_{50} values were obtained using GraphPad Prism software (La Jolla, CA) as described previously.^[39,40]

Selectivity Test for 24a. The inhibitory activities of **24a** against SIRT1 (0.2 μM), SIRT3 (0.2 μM), SIRT6 (0.2 μM), and SIRT7 (0.2 μM) were tested using AcIQF (50 μM) under the similar assay conditions as described above. Similarly, the inhibitory potency of **24a** to SIRT5 (0.2 μM) was determined using GluIQF (5 μM).

Crystallographic Analyses. The purified SIRT2 proteins (13 mg mL^{-1} in the buffer of 20 mM Tris/HCl pH 8.0, 150 mM NaCl) were co-crystallized with **1**, **24a**, or **24b** (100 mM stocks dissolved in 100% DMSO) at 4 $^{\circ}\text{C}$ by the hanging-drop vapor diffusion method. The SIRT2 proteins were preincubated for 2h on ice with inhibitors at a

molar ratio of 1:5 (SIRT2:Inhibitor). Then, 2 μ L crystallization drops composed of equal volumes (1 μ L) SIRT2 solution (13 mg mL⁻¹) and reservoir solution. The crystals that appeared within 7 days. The crystals were transferred to a cryo-protectant drop containing the reservoir, 19% glycerol and frozen in liquid nitrogen. X-ray diffraction data were obtained at the Shanghai Synchrotron Radiation Facility and processed using HKL2000. Initial phases were obtained by the molecular replacement method using the PHASER^[41] subroutine within PHENIX^[42], with the structure of SIRT2:SirReal2 (PDB ID 4RMG)^[22] as the search model. Crystallographic structure refinements were carried out by iterative rounds of model building using Coot^[43] and maximum likelihood restrained refinement using PHENIX. Crystallization conditions are in Table S2, and data collection and refinement statistics are in Table S3.

Cell Lines and Cell Culture. Human NSCLC cell lines were obtained from American Type Culture Collection (ATCC). All cell lines were cultured according to standard procedures and passaged for less than 6 months after resuscitation.

Western Blot Analysis. Whole-cell protein lysates were prepared as described previously.^[44,45] Proteins were separated by SDS-PAGE, and then transferred to polyvinylidene fluoride (PVDF) membranes (Millipore, USA), followed by immunoblot with antibodies. The following antibodies purchased from Abcam were used at a 1:1,000 dilution: anti-Sirt2, anti- α -tubulin, anti-AC- α -tubulin. The horseradish peroxidase- coupled secondary antibodies (Zhong Shan Golden Bridge Bio-technology, China) were used at 1:5,000. Antibody-antigen complexes were detected using the Enhanced Chemiluminescence System (Millipore, USA).

Cell Viability Assays. Cell viability was measured by MTT assays. Briefly, cells growing in 96-well plate were treated with DMSO vehicle or different concentrations of compounds for 72 h. Then 20 μ L of MTT reagent (5 mg/mL, Sigma, USA) was added to each well, and the plates were incubated at 37 °C for another 4 h. After that, the formazan crystals were dissolved with 20% acidified SDS (w/v) overnight, and absorbance was detected at 570 nm using Multiskan MK3 (Thermo Scientific, USA).

Colony Formation Assays. Cells were seeded in six-well plate at a density of 5,000 cells per well, and then treated with DMSO vehicle or the compounds for 2 weeks. The agents were replaced every 3 days. At the end of incubation, cells were fixed with methanol and stained with 0.05% crystal violet (w/v).

Cell Proliferation Assays. Cells growing in 96-well plate were treated with DMSO vehicle or the compounds for 48 h. EdU incorporation assay was conducted to determine the cell proliferation following the manufacturer's instruction (RIBOBIO, China). The images were captured using ArrayScan VTI HCS reader (Thermo Scientific, USA).

Apoptosis Assays. Cells were treated with DMSO vehicle or the compounds for 48 h and harvested. Then the apoptosis was detected using the Annexin V-FITC/PI apoptosis detection kit (KeyGEN Bio TECH, China) according to the manufacturer's protocol. The apoptosis profiles were analyzed by the FlowJo 10.0 software (Treestar Software, San Carlos, California, USA).

Wound Healing Assays. Cells were cultured to confluence in 12-well plate and wounded by scratching with a sterilized yellow pipette tip, followed by treatment with

DMSO vehicle or the compounds for 24 h. Pictures were taken by the OLYMPUS digital camera attached to a light microscope.

Transwell Invasion Assays. The Millicell Hanging Cell Culture Inserts (Millipore, USA) were inserted in the 24-well plate and pre-coated with 50 μ L diluted Matrigel (BD Biosciences, USA). H441 cells were suspended in serum-free RPMI1640 medium and seeded in the upper chamber at a density of $5 \times 10^4/100 \mu$ L. Then another serum-free medium containing DMSO vehicle or the compounds was added to each upper chamber. The lower chambers were filled with 500 μ L RPMI1640 complete medium. After incubation for 48 h, the invaded cells were fixed with methanol and stained with 0.05% crystal violet (w/v).

Supporting Information

The Supporting Information is available free of charge on the ACS Publications website at DOI: 10.1021/acs.jmedchem.0000000.

The details of chemical synthesis for intermediates, crystallographic data collection and refinement statistics, additional figures and tables, and $^1\text{H}/^{13}\text{C}$ NMR spectra.

Accession Codes

The coordinate data for the SIRT:1 (PDB ID: 5YQL), SIRT:24a (PDB ID: 5YQO), and SIRT:24b (PDB ID: 5YQN) complex structures have been deposited in the Protein Data Bank. Authors will release the atomic coordinates and experimental data

upon article publication.

Corresponding Author

* Guo-Bo Li: phone, +86-28-85503235; E-mail, liguobo@scu.edu.cn.

* Qiang Chen: phone, +86-28-85502796; E-mail, qiang_chen@scu.edu.cn.

ORCID

Guo-Bo Li: 0000-0002-4915-6677

Qiang Chen: 0000-0002-2398-4482

Author Contributions

¹L.-L. Yang, H.-L. Wang, and L. Zhong contributed equally to this work.

Notes

The authors declare no competing financial interest.

Abbreviations Used

KDAC, lysine deacetylase; NAD⁺, nicotinamide adenine dinucleotide; HDAC, histone deacetylase; SIRT, sirtuin; IC₅₀, half-maximal inhibitory concentration; SAR, structure-activity relationship; ASU, asymmetric unit; NSCLC, non-small cell lung cancer.

ACKNOWLEDGMENTS

This work was supported by the funds from the National Natural Science Foundation (Grant Nos: 81703355, 81501368, 81672722, 81502989 and 81702286) and the Scientific Research Foundation of Sichuan University (Grant No.: 20822041A4193). The authors thank the staff of BL19U1 beamline of the National Center for Protein Science Shanghai at Shanghai Synchrotron Radiation Facility for assistance during data collection.

References

- [1] G.S. Hailu, D. Robaa, M. Forgione, W. Sippl, D. Rotili, A. Mai, Lysine Deacetylase Inhibitors in Parasites: Past, Present, and Future Perspectives, *J. Med. Chem.* 60 (2017) 4780-4804.
- [2] A. Chalkiadaki, L. Guarente, The multifaceted functions of sirtuins in cancer, *Nat. Rev. Cancer* 15 (2015) 608-624.
- [3] M.W. Van Dyke, Lysine Deacetylase (KDAC) Regulatory Pathways: an Alternative Approach to Selective Modulation, *ChemMedChem* 9 (2014) 511-522.
- [4] B. Chen, W. Zang, J. Wang, Y. Huang, Y. He, L. Yan, J. Liu, W. Zheng, The chemical biology of sirtuins, *Chem. Soc. Rev.* 44 (2015) 5246-5264.
- [5] R.H. Houtkooper, E. Pirinen, J. Auwerx, Sirtuins as regulators of metabolism and healthspan, *Nat. Rev. Mol. Cell Biol.* 13 (2012) 225-238.
- [6] T.M. Liu, N. Shyh-Chang, SIRT2 and glycolytic enzyme acetylation in pluripotent stem cells, *Nat. Cell Biol.* 19 (2017) 412-414.
- [7] J. Chen, A.W.H. Chan, K.-F. To, W. Chen, Z. Zhang, J. Ren, C. Song, Y.-S. Cheung, P.B.S. Lai, S.-H. Cheng, M.H.L. Ng, A. Huang, *et al.*, SIRT2 overexpression in hepatocellular carcinoma mediates epithelial to mesenchymal transition by protein kinase B/glycogen synthase kinase-3 β / β -catenin signaling, *Hepatology* 57 (2013) 2287-2298.

- [8] H. Jing, J. Hu, B. He, Yashira L. Negrón Abril, J. Stupinski, K. Weiser, M. Carbonaro, Y.-L. Chiang, T. Southard, P. Giannakakou, Robert S. Weiss, H. Lin, A SIRT2-Selective Inhibitor Promotes c-Myc Oncoprotein Degradation and Exhibits Broad Anticancer Activity, *Cancer Cell* 29 (2016) 297-310.
- [9] J.-H. Lee, B. Yang, A.J. Lindahl, N. Damaschke, M.D. Boersma, W. Huang, E. Corey, D.F. Jarrard, J.M. Denu, Identifying Dysregulated Epigenetic Enzyme Activity in Castrate-Resistant Prostate Cancer Development, *ACS Chem. Biol.* 12 (2017) 2804–2814.
- [10] W. Zhou, T.K. Ni, A. Wronski, B. Glass, A. Skibinski, A. Beck, C. Kuperwasser, The SIRT2 Deacetylase Stabilizes Slug to Control Malignancy of Basal-like Breast Cancer, *Cell Rep.* 17 (2016) 1302-1317.
- [11] M. Gertz, F. Fischer, G.T. Nguyen, M. Lakshminarasimhan, M. Schutkowski, M. Weyand, C. Steegborn, Ex-527 inhibits Sirtuins by exploiting their unique NAD⁺-dependent deacetylation mechanism, *Proc. Natl. Acad. Sci. U.S.A.* 110 (2013) E2772-2781.
- [12] J.S. Disch, G. Evindar, C.H. Chiu, C.A. Blum, H. Dai, L. Jin, E. Schuman, K.E. Lind, S.L. Belyanskaya, J. Deng, F. Coppo, L. Aquilani, *et al.*, Discovery of Thieno[3,2-d]pyrimidine-6-carboxamides as Potent Inhibitors of SIRT1, SIRT2, and SIRT3, *J. Med. Chem.* 56 (2013) 3666-3679.
- [13] H. Cui, Z. Kamal, T. Ai, Y. Xu, S.S. More, D.J. Wilson, L. Chen, Discovery of Potent and Selective Sirtuin 2 (SIRT2) Inhibitors Using a Fragment-Based Approach, *J. Med. Chem.* 57 (2014) 8340-8357.
- [14] T. Seifert, M. Malo, T. Kokkola, K. Engen, M. Fridén-Saxin, E.A.A. Wallén, M. Lahtela-Kakkonen, E.M. Jarho, K. Luthman, Chroman-4-one- and Chromone-Based Sirtuin 2 Inhibitors with Antiproliferative Properties in Cancer Cells, *J. Med. Chem.* 57 (2014) 9870-9888.
- [15] P.R. Tatum, H. Sawada, Y. Ota, Y. Itoh, P. Zhan, N. Ieda, H. Nakagawa, N. Miyata, T. Suzuki, Identification of novel SIRT2-selective inhibitors using a click chemistry approach, *Bioorg. Med. Chem. Lett.* 24 (2014) 1871-1874.
- [16] M.A. Khanfar, L. Quinti, H. Wang, J. Nobles, A.G. Kazantsev, R.B. Silverman,

- Design and Evaluation of 3-(Benzylthio)benzamide Derivatives as Potent and Selective SIRT2 Inhibitors, *ACS Med. Chem. Lett.* 6 (2015) 607-611.
- [17] T. Yang, X. Chen, H.-x. Jin, G. Sethi, M.-L. Go, Functionalized tetrahydro-1H-pyrido[4,3-b]indoles: A novel chemotype with Sirtuin 2 inhibitory activity, *Eur. J. Med. Chem.* 92 (2015) 145-155.
- [18] T. Ai, D.J. Wilson, S.S. More, J. Xie, L. Chen, 5-((3-Amidobenzyl)oxy)nicotinamides as Sirtuin 2 Inhibitors, *J. Med. Chem.* 59 (2016) 2928-2941.
- [19] S. Moniot, M. Forgione, A. Lucidi, G.S. Hailu, A. Nebbioso, V. Carafa, F. Baratta, L. Altucci, N. Giacché, D. Passeri, R. Pellicciari, A. Mai, *et al.*, Development of 1,2,4-Oxadiazoles as Potent and Selective Inhibitors of the Human Deacetylase Sirtuin 2: Structure–Activity Relationship, X-ray Crystal Structure, and Anticancer Activity, *J. Med. Chem.* 60 (2017) 2344-2360.
- [20] E. Therrien, G. Larouche, N. Nguyen, J. Rahil, A.-M. Lemieux, Z. Li, M. Fournel, T.P. Yan, A.-J. Landry, S. Lefebvre, J.J. Wang, K. MacBeth, *et al.*, Discovery of bicyclic pyrazoles as class III histone deacetylase SIRT1 and SIRT2 inhibitors, *Bioorg. Med. Chem. Lett.* 25 (2015) 2514-2518.
- [21] M. Schiedel, T. Rumpf, B. Karaman, A. Lehotzky, J. Olah, S. Gerhardt, J. Ovadi, W. Sippl, O. Einsle, M. Jung, Aminothiazoles as Potent and Selective Sirt2 Inhibitors: A Structure-Activity Relationship Study, *J. Med. Chem.* 59 (2016) 1599-1612.
- [22] T. Rumpf, M. Schiedel, B. Karaman, C. Roessler, B.J. North, A. Lehotzky, J. Olah, K.I. Ladwein, K. Schmidtkunz, M. Gajer, M. Pannek, C. Steegborn, *et al.*, Selective Sirt2 inhibition by ligand-induced rearrangement of the active site, *Nat. Commun.* 6 (2015) 6263.
- [23] M. Schiedel, T. Rumpf, B. Karaman, A. Lehotzky, S. Gerhardt, J. Ovádi, W. Sippl, O. Einsle, M. Jung, Structure-Based Development of an Affinity Probe for Sirtuin 2, *Angew. Chem. Int. Ed.* 55 (2016) 2252-2256.
- [24] S. Sundriyal, S. Moniot, Z. Mahmud, S. Yao, P. Di Fruscia, C.R. Reynolds, D.T. Dexter, M.J.E. Sternberg, E.W.F. Lam, C. Steegborn, M.J. Fuchter,

- Thienopyrimidinone Based Sirtuin-2 (SIRT2)-Selective Inhibitors Bind in the Ligand Induced Selectivity Pocket, *J. Med. Chem.* 60 (2017) 1928-1945.
- [25] G.-B. Li, S. Ji, L.-L. Yang, R.-J. Zhang, K. Chen, L. Zhong, S. Ma, S.-Y. Yang, LEADOPT: An automatic tool for structure-based lead optimization, and its application in structural optimizations of VEGFR2 and SYK inhibitors, *Eur. J. Med. Chem.* 93 (2015) 523-538.
- [26] L. Yang, X. Ma, C. Yuan, Y. He, L. Li, S. Fang, W. Xia, T. He, S. Qian, Z. Xu, G. Li, Z. Wang, Discovery of 2-((4,6-dimethylpyrimidin-2-yl)thio)-N-phenylacetamide derivatives as new potent and selective human sirtuin 2 inhibitors, *Eur. J. Med. Chem.* 134 (2017) 230-241.
- [27] J.L. Feldman, K.E. Dittenhafer-Reed, N. Kudo, J.N. Thelen, A. Ito, M. Yoshida, J.M. Denu, Kinetic and Structural Basis for Acyl-Group Selectivity and NAD⁺ Dependence in Sirtuin-Catalyzed Deacylation, *Biochemistry* 54 (2015) 3037-3050.
- [28] I.V. Tetko, J. Gasteiger, R. Todeschini, A. Mauri, D. Livingstone, P. Ertl, V.A. Palyulin, E.V. Radchenko, N.S. Zefirov, A.S. Makarenko, V.Y. Tanchuk, V.V. Prokopenko, Virtual computational chemistry laboratory--design and description, *J. Comput. Aided Mol. Des.* 19 (2005) 453-463.
- [29] S. Moniot, M. Schutkowski, C. Steegborn, Crystal structure analysis of human Sirt2 and its ADP-ribose complex, *Journal of Structural Biology* 182 (2013) 136-143.
- [30] L. Yang, X. Ma, Y. He, C. Yuan, Q. Chen, G. Li, X. Chen, Sirtuin 5: a review of structure, known inhibitors and clues for developing new inhibitors, *Science China Life Sciences* 60 (2017) 249-256.
- [31] M. Pannek, Z. Simic, M. Fuszard, M. Meleshin, D. Rotili, A. Mai, M. Schutkowski, C. Steegborn, Crystal structures of the mitochondrial deacylase Sirtuin 4 reveal isoform-specific acyl recognition and regulation features, *Nat. Commun.* 8 (2017) 1513.
- [32] J. Du, Y. Zhou, X. Su, J.J. Yu, S. Khan, H. Jiang, J. Kim, J. Woo, J.H. Kim,

- B.H. Choi, B. He, W. Chen, *et al.*, Sirt5 is a NAD-dependent protein lysine demalonylase and desuccinylase, *Science* 334 (2011) 806-809.
- [33] X. Zhang, S. Khan, H. Jiang, M.A. Antonyak, X. Chen, N.A. Spiegelman, J.H. Shrimp, R.A. Cerione, H. Lin, Identifying the functional contribution of the defatty-acylase activity of SIRT6, *Nat. Chem. Biol.* 12 (2016) 614-620.
- [34] G. Hoffmann, F. Breitenbucher, M. Schuler, A.E. Ehrenhofer-Murray, A novel sirtuin 2 (SIRT2) inhibitor with p53-dependent pro-apoptotic activity in non-small cell lung cancer, *J. Biol. Chem.* 289 (2014) 5208-5216.
- [35] I. Grbesa, M.J. Pajares, E. Martinez-Terroba, J. Agorreta, A.M. Mikecin, M. Larrayoz, M.A. Idoate, K. Gall-Troselj, R. Pio, L.M. Montuenga, Expression of sirtuin 1 and 2 is associated with poor prognosis in non-small cell lung cancer patients, *PLoS One* 10 (2015) e0124670.
- [36] Z. Li, J. Huang, H. Yuan, Z. Chen, Q. Luo, S. Lu, SIRT2 inhibits non-small cell lung cancer cell growth through impairing Skp2-mediated p27 degradation, *Oncotarget* 7 (2016) 18927-18939.
- [37] L.L. Zhang, L. Zhan, Y.D. Jin, Z.L. Min, C. Wei, Q. Wang, Y.J. Chen, Q.M. Wu, X.M. Hu, Q. Yuan, SIRT2 mediated antitumor effects of shikonin on metastatic colorectal cancer, *Eur. J. Pharmacol.* 797 (2017) 1-8.
- [38] Q. Zuo, W. Wu, X. Li, L. Zhao, W. Chen, HDAC6 and SIRT2 promote bladder cancer cell migration and invasion by targeting cortactin, *Oncol. Rep.* 27 (2012) 819-824.
- [39] G.-B. Li, M.I. Abboud, J. Brem, H. Someya, C.T. Lohans, S.-Y. Yang, J. Spencer, D.W. Wareham, M.A. McDonough, C.J. Schofield, NMR-filtered virtual screening leads to non-metal chelating metallo- β -lactamase inhibitors, *Chem. Sci.* 8 (2017) 928-937.
- [40] G.-B. Li, J. Brem, R. Lesniak, M.I. Abboud, C.T. Lohans, I.J. Clifton, S.-Y. Yang, J.-C. Jimenez-Castellanos, M.B. Avison, J. Spencer, M.A. McDonough, C.J. Schofield, Crystallographic analyses of isoquinoline complexes reveal a new mode of metallo- β -lactamase inhibition, *Chem. Commun.* 53 (2017) 5806-5809.

- [41] A.J. McCoy, R.W. Grosse-Kunstleve, P.D. Adams, M.D. Winn, L.C. Storoni, R.J. Read, Phaser crystallographic software, *J. Appl. Crystallogr.* 40 (2007) 658-674.
- [42] P.D. Adams, P.V. Afonine, G. Bunkoczi, V.B. Chen, I.W. Davis, N. Echols, J.J. Headd, L.W. Hung, G.J. Kapral, R.W. Grosse-Kunstleve, A.J. McCoy, N.W. Moriarty, *et al.*, PHENIX: a comprehensive Python-based system for macromolecular structure solution, *Acta Crystallogr. D Biol. Crystallogr.* 66 (2010) 213-221.
- [43] P. Emsley, K. Cowtan, Coot: model-building tools for molecular graphics, *Acta Crystallogr D Biol Crystallogr* 60 (2004) 2126-2132.
- [44] L.-L. Yang, G.-B. Li, S. Ma, C. Zou, S. Zhou, Q.-Z. Sun, C. Cheng, X. Chen, L.-J. Wang, S. Feng, L.-L. Li, S.-Y. Yang, Structure–activity relationship studies of pyrazolo [3, 4-d] pyrimidine derivatives leading to the discovery of a novel multikinase inhibitor that potently inhibits FLT3 and VEGFR2 and evaluation of its activity against acute myeloid leukemia in vitro and in vivo, *J. Med. Chem.* 56 (2013) 1641-1655.
- [45] G.-B. Li, S. Ma, L.-L. Yang, S. Ji, Z. Fang, G. Zhang, L.-J. Wang, J.-M. Zhong, Y. Xiong, J.-H. Wang, S.-Z. Huang, L.-L. Li, *et al.*, Drug Discovery against Psoriasis: Identification of a New Potent FMS-like Tyrosine Kinase 3 (FLT3) Inhibitor, 1-(4-((1H-Pyrazolo[3,4-d]pyrimidin-4-yl)oxy)-3-fluorophenyl)-3-(5-(tert-butyl)isoxazol-3-yl)urea, That Showed Potent Activity in a Psoriatic Animal Model, *J. Med. Chem.* 59 (2016) 8293-8305.

- SAR studies reveal potent, selective SIRT2 inhibitors
- Crystallographic analyses reveal **24a** mimics the myristoylated substrates.
- **24a** elevates the acetylation level of α -tubulin in H441 cells.
- **24a** restrains cell growth through inhibiting cellular proliferation.
- **24a** suppresses the migration and invasion of H441 cells.